Global impact of mineral dust on cloud droplet number concentration

Vlassis A. Karydis[1], Alexandra P. Tsimpidi[1], Sara Bacer[1], Andrea Pozzer[1],
Athanasios Nenes[2,3,4] and Jos Lelieveld[1,5]

[1]Max Planck Institute for Chemistry, Mainz, 55128, DE
[2]Georgia Institute of Technology, Atlanta, GA, 30332, USA
[3]National Observatory of Athens, Palea Penteli, 15236, GR
[4]Foundation for Research and Technology Hellas, Patras, 26504, GR
[5]The Cyprus Institute, Nicosia, 1645, CY

Abstract

The importance of wind-blown mineral dust for cloud droplet formation is studied by considering *i)* the adsorption of water on the surface of insoluble particles, *ii)* the particle coating by soluble material (due to atmospheric aging) which augments cloud condensation nuclei (CCN) activity, and *iii)* the effect of dust on inorganic aerosol concentrations through thermodynamic interactions with mineral cations. The ECHAM5/MESSy Atmospheric Chemistry (EMAC) model is used to simulate the composition of global atmospheric aerosol; the ISORROPIA-II thermodynamic equilibrium model treats the interactions of K^+-Ca^{2+}-Mg^{2+}-NH_4^+-Na^+-SO_4^{2-}-NO_3^--Cl^--H_2O aerosol with gas-phase inorganic constituents. Dust is considered a mixture of inert material with reactive minerals; emissions are calculated online by taking into account the soil particle size distribution and chemical composition of different deserts worldwide. The impact of dust on droplet formation is treated through the "unified dust activation parameterization" that considers the inherent hydrophilicity from adsorption and acquired hygroscopicity from soluble salts during aging. Our simulations suggest that the presence of dust increases cloud droplet number concentrations (CDNC) over major deserts (e.g., up to 20% over the Sahara and Taklimakan Deserts) and decreases CDNC over polluted areas (e.g., up to 10% over southern Europe and 20% over northeastern Asia). This leads to a global net decrease of CDNC by 11%. The adsorption activation of insoluble aerosols and the mineral dust chemistry are shown to be equally important for the cloud droplet formation over the main desserts, e.g., by considering these effects CDNC increases by 20% over the Sahara. Remote from deserts the application of adsorption theory is critically important since the increased water uptake by the large aged dust particles (i.e., due to the added hydrophilicity by the soluble coating) reduce the maximum supersaturation

Atmospheric
Chemistry
and Physics
Discussions

39   and thus the cloud droplet formation from the smaller anthropogenic particles (e.g.,

40   CDNC decreases by 10% over southern Europe and 20% over northeastern Asia by

41   applying adsorption theory). The global average CDNC decreases by 10% by

42   considering adsorption activation, while changes are negligible when accounting for

43   the mineral dust chemistry. Sensitivity simulations indicate that CDNC is also

44   sensitive to the mineral dust mass and inherent hydrophilicity, and not to the chemical

45   composition of the emitted dust.

46

47   **1.   Introduction**

48   Atmospheric aerosols from anthropogenic and natural sources adversely affect

49   human health and influence the Earth's climate, both directly and indirectly

50   (Haywood and Boucher, 2000; Lohmann and Feichter, 2005; Andreae and Rosenfeld,

51   2008; IPCC, 2013; Kushta et al., 2014; Lelieveld et al., 2015). The direct climate

52   effect refers to the influence of aerosols on the radiative budget of Earth's atmosphere

53   by scattering and absorbing solar radiation (Seinfeld and Pandis, 2006). The indirect

54   effects include the ability of aerosols to affect the cloud optical thickness and

55   scattering properties of clouds (Twomey, 1974) as well as the cloud lifetime and

56   precipitation (Albrecht, 1989). The scientific interest in aerosol-cloud-climate

57   interactions initially focused on anthropogenic pollutants (e.g., sulfate) and to a lesser

58   extent on naturally emitted aerosols (e.g., sea salt). However, among atmospheric

59   aerosols, mineral dust is of particular importance since it is globally dominant in

60   terms of mass concentration in the atmosphere (Grini et al., 2005; Zender and Kwon,

61   2005) and can influence cloud and precipitation formation (Levin et al., 2005; Yin

62   and Chen, 2007; Karydis et al., 2011; Rosenfeld et al., 2011; Kallos et al., 2014).

63   Additionally, dust alone is responsible for more than 400,000 premature deaths per

64   year (Giannadaki et al., 2014).

65   Freshly emitted dust is considered insoluble. Reports of hygroscopic growth

66   measurements of dust particles indicate solubility to be very low, which together with

67   the observed cloud condensation nuclei (CCN), has been attributed to soluble ions

68   present in the particles (Gustafsson et al., 2005; Herich et al., 2009; Koehler et al.,

69   2009; Garimella et al., 2014). Chemistry – climate models (CCMs) typically use

70   Köhler theory to describe droplet formation from dust, which assumes that the CCN

71   activity depends solely on their curvature effect and the fraction of soluble material on

72   the particle (Smoydzin et al., 2012). However, mineral dust can adsorb water which

73   results in a surface film of water with reduced activity (Sorjamaa and Laaksonen,

74   2007), and promote the formation of cloud droplets at cloud-relevant supersaturation,

75   even of freshly emitted and chemically unprocessed dust particles (Sorjamaa and

76   Laaksonen, 2007; Kumar et al., 2009a). Kumar et al. (2009a) emphasized the

77   importance of including water adsorption effects in describing the hygroscopic growth

78   of mineral aerosols, which was then included in a droplet formation parameterization

79   (Kumar et al. (2009b) for use in models. Evidence on the importance of adsorption

80   activation of dust particles is discussed in Kumar et al. (2011b; 2011a) for dry- and

81   wet-generated clays and mineral dusts representative of major regional dust sources

82   (North Africa, East Asia and North America). Adsorption activation was also found to

83   be important for volcanic ashes (Lathem et al., 2011). The observed hygroscopicity

84   could not be attributed to the soluble ions present, but rather to the strong water vapor

85   adsorption on the particle surface. Furthermore, the surface fractal dimension derived

86   from dust and ash critical supersaturation data agrees well with previous methods

87   based on measurements of nitrogen adsorption, which contribute strong evidence for

88   adsorption effects on water activity and droplet activation (Laaksonen et al., 2016),

89   despite concerns raised by Garimella et al. (2014) on multiple charging effects on the

90   work of Kumar et al. (2011b). Hatch et al. (2014) provided an alternative approach for

91   parameterizing CCN activation of fresh atmospheric mineral aerosol. This approach

92   was based on experimental water adsorption measurements on mineral clays

93   compared to CCN measurements used by Kumar et al. (2011b), which require

94   corrections for multiply charged particles and non-sphericity. Despite differences in

95   the adsorption parameters reported from the above two studies, the adsorption derived

96   CCN activities were quite similar and in excellent agreement. Based on these

97   findings, Karydis et al. (2011) integrated the Kumar et al. (2009b) parameterization

98   into the Global Modeling Initiative (GMI) chemical transport model (Considine et al.,

99   2005) and found that insoluble mineral dust can contribute up to 24% of the cloud

100   droplet number downwind of arid areas. Subsequently, the Kumar et al. (2009b)

101   parameterization has been integrated in a number of global and regional models and

102   applied to investigate the impact of mineral dust on warm cloud formation (Bangert et

103   al., 2012; Karydis et al., 2012; Gantt et al., 2014; Zhang et al., 2015).

104   Soluble inorganic ions like Ca^{+2}, Mg^{+2}, Na^+, and K^+ that exist on the surface of

105   mineral dust particles can participate in heterogeneous chemical reactions with acids

106   such as HNO_3 and HCl. Furthermore, dust particles can provide reaction sites for the

Atmospheric
Chemistry
and Physics
Discussions

107   SO_2 oxidation into H_2SO_4. These processes result in the coating of dust particles by

108   soluble material, which augments the hygroscopicity of dust and therefore its ability

109   to act as CCN (Kelly et al., 2007). On the other hand, highly oxidized, soluble organic

110   species, particularly including carboxylic acid groups (e.g., oxalic acid), can interact

111   with particles dominated by di-valent salts (e.g., $CaCl_2$) and strongly decrease their

112   hygroscopicity (Drozd et al., 2014). Due to their relatively large size, chemically aged

113   dust particles can act as giant CCN, enhancing precipitation as they efficiently collect

114   moisture and grow at the expense of smaller droplets (Feingold et al., 1999; Levin et

115   al., 2005). In addition, giant CCN compete with the submicron particles for water

116   vapor, potentially reducing supersaturation and cloud droplet formation (Barahona et

117   al., 2010; Betancourt and Nenes, 2014b; Betancourt and Nenes, 2014a). Soluble

118   coatings on dust are mostly evident in the atmosphere after long-range transport of

119   dust plumes. Anthropogenic NO_3^- and SO_4^{2-} mainly contribute to the chemical aging

120   of dust over continents while sea salt derived Cl^- is more important over oceans

121   (Sullivan et al., 2007; Fountoukis et al., 2009; Dall'Osto et al., 2010; Tobo et al.,

122   2010; Bougiatioti et al., 2016b; Weber et al., 2016). Apart from the gas phase

123   composition, the chemical processing of dust also depends on its chemical

124   composition and thus on the source region (Sullivan et al., 2009; Karydis et al., 2016).

125   Several studies have revealed that Saharan dust can be efficiently transported over the

126   Mediterranean basin where it can acquire significant soluble coatings (mostly sea salt

127   and sulfate) resulting in the enhancement of its hygroscopicity and CCN activity

128   (Wurzler et al., 2000; Falkovich et al., 2001; Smoydzin et al., 2012; Abdelkader et al.,

129   2015). Twohy et al. (2009) have shown that Saharan dust often acts as CCN over the

130   eastern North Atlantic and significantly contributes to cloud formation west of Africa.

131   Begue et al. (2015) analyzed a case of possible mixing of European pollution aerosols

132   with Saharan dust transported over northern Europe, and found that aged Saharan dust

133   was sufficiently soluble to impact the hygroscopic growth and cloud droplet

134   activation over the Netherlands. Asian dust has also been reported to have a

135   considerable impact on cloud formation after being transported over long distances

136   and mixed with soluble materials (Perry et al., 2004; Roberts et al., 2006; Sullivan et

137   al., 2007; Ma et al., 2010; Stone et al., 2011; Yamashita et al., 2011).

138   Despite the importance of mineral dust aerosol chemistry for accurately predicting

139   the aerosol hygroscopicity changes that accompany these reactions, most

140   thermodynamic models used in global studies lack a realistic treatment of crustal

141 species, e.g., assuming that mineral dust is chemically inert (Liao et al., 2003; Martin

142 et al., 2003; Koch et al., 2011; Leibensperger et al., 2011). Only few global studies

143 have accounted for the thermodynamic interactions of crustal elements with inorganic

144 aerosol components (Feng and Penner, 2007; Fairlie et al., 2010; Xu and Penner,

145 2012; Hauglustaine et al., 2014; Karydis et al., 2016). Most of these models either

146 neglect the impact of dust on cloud droplet formation or apply simplified assumptions

147 about the CCN activity of dust, e.g., they convert "hydrophobic" dust to "hydrophilic"

148 dust by applying a constant κ-hygroscopicity (e.g., 0.1) and use Köhler theory to

149 describe cloud droplet activation. However, accounting for both the inherent

150 hydrophilicity of dust and the acquired hygroscopicity from soluble salts could

151 improve the predictive capability of CCMs. For this purpose, Kumar et al. (2011a)

152 presented a "unified dust activation framework" (UAF) to treat the activation of dust

153 with substantial amounts of soluble material by considering the effects of adsorption

154 (due to the hydrophilicity of the insoluble core) and absorption (due to the

155 hygroscopicity of the soluble coating) on CCN activity. Karydis et al. (2011) provided

156 a first estimate of aged dust contribution to global CCN and cloud droplet number

157 concentration (CDNC) by using the UAF. They found that coating of dust by

158 hygroscopic salts can cause a twofold enhancement of its contribution to CCN. On the

159 other hand, aged dust can be substantially depleted due to in-cloud supersaturation

160 and eventually reduce the CDNC. Bangert et al (2012) investigated the impact of

161 Saharan dust on cloud droplet formation over western Europe and found only a slight

162 increase in calculated CDNC. However, these studies did not include thermodynamic

163 interactions of mineral dust with sea salt and anthropogenic pollutants. Instead, a

164 prescribed fraction of mineral dust that is coated with ammonium sulfate was used to

165 represent the aged dust.

166   The present work aims at advancing previous studies on dust influences of cloud

167 droplet formation by comprehensively considering *i*) the adsorption of water on the

168 surface of insoluble dust particles, *ii*) the coating of soluble material on the surface of

169 mineral particles which augments their CCN activity, and, *iii*) the effects of dust on

170 the inorganic soluble fraction of dust through thermodynamic interactions of semi-

171 volatile inorganic species and sulfate with mineral cations. The ECHAM5/MESSy

172 Atmospheric Chemistry (EMAC) model (Jöckel et al., 2006) is used to simulate

173 aerosol processes, while the "unified dust activation framework" (Karydis et al., 2011;

174 Kumar et al., 2011a) is applied to calculate the CCN spectra and droplet number

175 concentration, by explicitly accounting for the inherent hydrophilicity from adsorption

176 and acquired hygroscopicity from soluble salts by dust particles from atmospheric

177 aging. Mineral dust chemistry has been taken into account by using the

178 thermodynamic equilibrium model ISORROPIA II (Fountoukis and Nenes, 2007).

179 Dust emissions are calculated online by an advanced dust emission scheme which

180 accounts for the soil particle size distribution (Astitha et al., 2012) and chemical

181 composition (Karydis et al., 2016) of different deserts worldwide. The sensitivity of

182 the simulations to the emitted dust aerosol load, the mineral dust chemical

183 composition and the inherent hydrophilicity of mineral dust is also considered.

184
185 **2. Model Description**

186
187 **2.1 EMAC Model**

188 We used the ECHAM5/MESSy Atmospheric Chemistry (EMAC) model (Jöckel et

189 al., 2006) which uses the Modular Earth Submodel System (MESSy2) (Jöckel et al.,

190 2010) to connect submodels that describe the lower and middle atmosphere processes

191 with the 5th generation European Centre - Hamburg (ECHAM5) general circulation

192 model (GCM) as a dynamical core (Röckner et al., 2006). EMAC has been

193 extensively described and evaluated against in-situ observations and satellite

194 retrievals (de Meij et al., 2012; Pozzer et al., 2012; Tsimpidi et al., 2014; Karydis et

195 al., 2016). The spectral resolution of the EMAC model used in this study is T63L31,

196 corresponding to a horizontal grid resolution of approximately $1.9^{\circ} \times 1.9^{\circ}$ and 31

197 vertical layers between the surface and 10 hPa (i.e. 25 km altitude). EMAC is applied

198 for 2 years covering the period 2004-2005 and the first year is used as spin-up.

199 EMAC simulates the gas phase species through the MECCA submodel (Sander et

200 al., 2011). Aerosol microphysics are calculated by the GMXe module (Pringle et al.,

201 2010). The organic aerosol formation and chemical aging is calculated by the

202 ORACLE submodel (Tsimpidi et al., 2014). The CLOUD submodel (Röckner et al.,

203 2006) calculates the cloud cover as well as cloud micro-physics and precipitation of

204 large scale clouds (i.e., excluding convective clouds). The wet and dry deposition are

205 calculated by the SCAV (Tost et al., 2006) and the DRYDEP (Kerkweg et al., 2006)

206 sub-models.

207 The inorganic aerosol composition is computed with the ISORROPIA-II

208 (http://isorropia.eas.gatech.edu) thermodynamic equilibrium model (Fountoukis and

Atmospheric
Chemistry
and Physics
Discussions

209   Nenes, 2007) with updates as discussed in Capps et al. (2012). ISORROPIA-II

210   calculates the gas-liquid-solid equilibrium partitioning of the K^+-Ca^{2+}-Mg^{2+}-NH_4^+-

211   Na^+-SO_4^{2-}-NO_3^--Cl^--H_2O aerosol system. Potassium, calcium, magnesium, and

212   sodium are assumed to exist in the form of $Ca(NO_3)_2$, $CaCl_2$, $CaSO_4$, $KHSO_4$, K_2SO_4,

213   KNO_3, KCl, $MgSO_4$, $Mg(NO_3)_2$, $MgCl_2$, $NaHSO_4$, Na_2SO_4, $NaNO_3$, $NaCl$ in the solid

214   phase and Ca^{2+}, K^+, Mg^{2+}, Na^+ in the aqueous phase. More details about the EMAC

215   model set up used in this study can be found in Karydis et al. (2016).

216

217   **2.2 CCN Activity and Cloud Droplet Formation Parameterization**

218   The equilibrium supersaturation, s, over the surface of a water droplet containing a

219   solute particle (i.e., without any insoluble material present) is calculated using the

220   hygroscopicity parameter, κ, based on κ-Köhler theory (Petters and Kreidenweis,

221   2007):

222
$$s = \frac{4\sigma M_w}{RT\rho_w D_P} - \frac{D_{dry}^3 \kappa}{D_P^3} \quad (1)$$

223   where D_{dry} is the dry CCN diameter, D_p is the droplet diameter, σ is the CCN surface

224   tension at the point of activation, ρ_w is the water density, M_w is the molar mass of

225   water, R is the universal gas constant, and T is the average column temperature.

226   For insoluble particles (e.g., pristine mineral dust), the multilayer Frenkel-Halsey-

227   Hill (FHH) adsorption isotherm model (Sorjamaa and Laaksonen, 2007) is used,

228   which contains two adjustable parameters (A_{FHH} and B_{FHH}) that describe the

229   contribution of water vapor adsorption on CCN activity. In this case, the equation

230   describing the equilibrium supersaturation over the surface of a water droplet is given

231   by (Kumar et al., 2009b):

232
$$s = \frac{4\sigma M_w}{RT\rho_w D_P} - A_{FHH}\left(\frac{D_P - D_{dry}}{2D_w}\right)^{-B_{FHH}} \quad (2)$$

233   where D_w is the diameter of a water molecule. The adsorption parameter A_{FHH}

234   represents the interactions between the first water monolayer and the dust surface.

235   B_{FHH} expresses the long range interactions of additional adsorbed water layers with

236   the dust surface. Kumar et al. (2011b) tested a wide range of fresh unprocessed

237   regional dust samples and minerals and found that one set of the FHH parameters

Atmospheric
Chemistry
and Physics
Discussions

Open Access

238   (A_{FHH} =2.25±0.75, B_{FHH} =1.20±0.10) adequately reproduces the measured CCN

239   activity for all dust types considered.

240   To account for the coating of soluble material on the surface of mineral dust, the

241   "unified activation framework" (Karydis et al., 2011; Kumar et al., 2011a) is used,

242   which describes the water vapor supersaturation over an aerosol particle consisting of

243   insoluble core with a soluble coating:

244
$$s = \frac{4\sigma M_w}{RT\rho_w D_P} - \frac{\varepsilon_s D_{dry}^3 \kappa}{\left(D_P^3 - \varepsilon_i D_{dry}^3\right)} - A_{FHH}\left(\frac{D_P - \varepsilon_i^{1/3} D_{dry}}{2D_w}\right)^{-B_{FHH}} \quad (3)$$

245   where ε_i is the insoluble volume fraction and ε_s is the soluble volume fraction. Eq. 3

246   takes into account both the inherent hydrophilicity from adsorption expressed in the

247   third term of the equation and the acquired hygroscopicity from soluble salts by dust

248   particles expressed in the second term of the equation. The first term accounts for the

249   Kelvin effect. Noting that for a complete insoluble dust particle, i.e., as $\varepsilon_s \to 0$ and

250   $\varepsilon_i \to 1$, the UAF approaches FHH theory (Eq. 2).

251   Calculation of CDNC is carried out in two conceptual steps, one involving the

252   determination of the "CCN spectrum" (i.e., the number of CCN that can activate to

253   form droplets at a certain level of supersaturation), and another one determining the

254   maximum supersaturation, s_{max}, that develops in the ascending cloudy air parcels used

255   to represent droplet formation in EMAC. The CDNC is then the value of the CCN

256   spectrum at s_{max}.

257   The "CCN spectrum", $F^s(s)$, is computed following Kumar et al. (2009b) and

258   assumes that particles can be described either by KT or FHH theory. $F^s(s)$ for an

259   external mixture of lognormal particle size distributions is given by:

260
$$F^s(s) = \int_0^s n^s(s)\,ds = \sum_{i=1}^{n_m} \frac{N_i}{2}\, erfc\left[-\frac{\ln\left(\frac{s_{g,i}}{s}\right)}{x\sqrt{2}\ln(\sigma_i)}\right] \quad (4)$$

261   where s is the level of water vapor supersaturation, $n^s(s)$ is the critical

262   supersaturation distribution, $s_{g,i}$ is the critical supersaturation of the particle with a

263   diameter equal to the geometric mean diameter of the mode i, σ_i is the geometric

264   standard deviation for the mode i, and x is an exponent that depends on the

265   activation theory used. For modes following Köhler theory, $x = -\dfrac{3}{2}$ (Fountoukis and

266   Nenes, 2005), while for insoluble particles following FHH theory, x depends on

267   A_{FHH} and B_{FHH} (Kumar et al., 2009b). In the case of UAF x lies between the KT

268   and FHH-AT limits, and is determined from Eq. (3) by performing a power law fit

269   between s_g and D_{dry} as described in Kumar et al. (2011a). The calculation of s_g

270   involves determining the maximum of the relevant equilibrium curve in equilibrium

271   with the surrounding water vapor ($\left. \dfrac{ds}{dD_p} \right|_{D_p = D_g} = 0$ in Eqs. 1-3). Once D_g is determined,

272   it can be substituted in Eqs. 1-3 to obtain s_g.

273   The maximum supersaturation, s_{max}, in the ascending parcel is calculated from an

274   equation that expresses the supersaturation tendency in cloudy air parcels, which at

275   the point of maximum supersaturation becomes (Nenes and Seinfeld, 2003; Barahona

276   and Nenes, 2007)

$$\frac{2aV}{\pi \gamma \rho_w} - G s_{max} I(0, s_{max}) = 0 \qquad (5)$$

278   where V is the updraft velocity (i.e., not including convection) calculated online by

279   assuming that the sub-grid vertical velocity variability is dominated by the turbulent

280   transports and by choosing the root-mean-square value of the GCM model-generated

281   turbulent kinetic energy (TKE) as a measure. Based on this assumption, the in-cloud

282   updraft velocity can be expressed as $V = {}^{-}V + 0.7 \sqrt{TKE}$, where ${}^{-}V$ is the GCM-

283   resolved large scale updraft velocity (Lohmann et al., 1999a; Lohmann et al., 1999b).

284   Following Morales and Nenes (2010), V can be considered as a "characteristic updraft

285   velocity" which yields CDNC value representative of integration over a probability

286   density function (PDF) of updraft velocity. Morales and Nenes (2010) have shown

287   that this assumption applies well to large scale clouds (i.e., stratocumulus), which are

288   the type of clouds described by the CLOUD sub-model in EMAC. a, γ, G in Eq. (5)

289   are parameters defined in Nenes and Seinfeld (2003). $I(0, s_{max})$ is the "condensation

290   integral" which expresses the condensational depletion of supersaturation upon the

291   growing droplets at the point of s_{max} in the cloud updraft. It is expressed as the sum of

292   two terms:

Atmospheric
Chemistry
and Physics
Discussions

293

$$I\left(0, s_{\max}\right) = I_K\left(0, s_{\max}\right) + I_{FHH}\left(0, s_{\max}\right) \quad (6)$$

295

296   The first term on the right hand side of Eq. (6), $I_K\left(0, s_{\max}\right)$, describes the contribution

297   from particles that follow the Köhler theory and is calculated using the revisited

298   population splitting approach of Betancourt and Nenes (2014a). The second term,

299   $I_{FHH}\left(0, s_{\max}\right)$, represents the contribution of freshly emitted or aged dust particles to

300   the condensation integral and is represented in Kumar et al. (2009b) and Karydis et al.

301   (2011). Once $s_{\max}$ is determined by numerically solving Eq. (5), the number of cloud

302   droplets that form in the parcel, N_d, is obtained from the "CCN spectrum" (Eq. (4))

303   computed for $s_{\max}$, i.e., $N_d = F\left(s_{\max}\right)$.

304

305   **2.3 Aerosol Precursor Emissions**

306   Dust emission fluxes are calculated online by an advanced dust flux scheme

307   developed by Astitha et al. (2012). This scheme uses an explicit geographical

308   representation of the airborne soil particle size distribution based on soil

309   characteristics in every grid cell. Emissions of crustal species (Ca^{2+}, Mg^{2+}, K^+, Na^+)

310   are estimated as a fraction of mineral dust emissions based on the chemical

311   composition of the emitted soil particles in every grid cell (Karydis et al., 2016).

312   Emissions of sea spray aerosols are based on the offline monthly emission data set of

313   AEROCOM (Dentener et al., 2006) assuming a composition of 55% Cl^-, 30.6% Na^+,

314   7.7% SO_4^{2-}, 3.7% Mg^{2+}, 1.2% Ca^{2+}, 1.1% K^+ (Seinfeld and Pandis, 2006). The

315   CMIP5 RCP4.5 emission inventory (Clarke et al., 2007) is used for the anthropogenic

316   primary organic aerosol emissions from fossil fuel and biofuel combustion sources.

317   The open biomass burning emissions from savanna and forest fires are based on the

318   GFED v3.1 database (van der Werf et al., 2010). More details about the aerosol phase

319   emissions used by EMAC can be found in Karydis et al. (2016) and Tsimpidi et al.

320   (2016).

321   Related anthropogenic emissions of NO_x, NH_3, and SO_2, which represent the

322   gaseous precursors of the major inorganic components, are based on the monthly

323   emission inventory of EDGAR-CIRCE (Doering, 2009) distributed vertically as

324   presented in Pozzer et al. (2009). The natural emissions of NH_3 are based on the

Atmospheric
Chemistry
and Physics
Discussions

325   GEIA database (Bouwman et al., 1997). NO_x produced by lightning is calculated

326   online and distributed vertically based on the parameterization of Grewe et al. (2001).

327   The emissions of NO from soils are calculated online based on the algorithm of

328   Yienger and Levy (1995) as described in Ganzeveld et al. (2002). Eruptive and non-

329   eruptive volcanic degassing emissions of SO_2 are based on the AEROCOM data set

330   (Dentener et al., 2006). The oceanic DMS emissions are calculated online by the

331   AIRSEA submodel (Pozzer et al., 2006). More details about the gas phase emissions

332   used by EMAC can be found in Pozzer et al. (2012) and Karydis et al. (2016).

333

334   **3. Model Results and Evaluation**

335   **3.1 Model Predictions**

336   The annual and seasonal (during DJF and JJA) mean CDNC calculated by EMAC

337   with UAF implementation for the lowest model level at which clouds are formed

338   (centered at 940 mb) are shown in Figure 1. The calculated CDNC is mostly sensitive

339   to the cloud updraft velocity and the total aerosol number concentration (Karydis et

340   al., 2012), which are the main drivers of the s_{max} calculations. The annual mean

341   aerosol number concentration, updraft velocity, and s_{max} calculated by EMAC at 940

342   mb are shown in Figure 2. The calculated global annual mean CDNC at 940 mb is

343   231 cm^{-3}.

344   Over the continents, the predicted annual mean CDNC is 546 cm^{-3} and exceeds

345   1000 cm^{-3} over the industrialized areas of Europe, central and eastern Asia, and North

346   America. In these areas, the aerosol number concentration is high (exceeding 10,000

347   cm^{-3}; Figure 2a), while the calculated updraft velocities (0.5-1 m s^{-1}; Figure 2b) allow

348   the development of sufficiently high s_{max} (0.1-0.3%; Figure 2c) for the activation of

349   5% (over eastern China) to 15% (over central Europe) of the pollution aerosols into

350   cloud droplets. The simulated s_{max} is close to the estimated s_{max} (0.2%-0.5%) for

351   stratocumulus clouds based on data from continental air masses (Twomey and

352   Wojciechowski, 1968; Martin et al., 1993) indicating that the combination of aerosol

353   number concentration and updraft velocity in the model is realistic. While the aerosol

354   number concentration over the industrialized areas remains fairly constant throughout

355   the year, the updraft velocity is higher during the boreal winter (i.e., DJF) resulting in

356   a seasonal peak of CDNC during DJF (exceeding 2,000 cm^{-3}) over North America,

Atmospheric
Chemistry
and Physics
Discussions

357   Europe and eastern Asia (Figure 1b). The highest annual mean CDNC is calculated

358   over northern India (~2,000 cm^{-3}) where the model simulates highest aerosol

359   concentrations (~30,000 cm^{-3}). Over Southeast Asia and India, CDNC peaks during

360   JJA (exceeding 2,000 cm^{-3}; Figure 1c), affected by the East Asian Monsoon and the

361   high updraft velocities developed during the wet season. Relatively high CDNC

362   (annual mean of 300-700 cm^{-3}) are also calculated over the tropical regions of the

363   Southern Hemisphere which are influenced by biomass burning. Relatively low

364   values are calculated over the Congo Basin where the mean updraft velocity is

365   typically low (below 0.2 m s^{-1}) leading to low s_{max} (below 0.05%) and cloud droplet

366   activation (~300 cm^{-3}). Downwind of deserts, the calculated CDNC varies between

367   100 cm^{-3} (e.g., Patagonia, and Australian deserts) to 1,000 cm^{-3} (e.g., Sahara, Arabian,

368   Taklimakan, Gobi and Atacama). In the vicinity of the Sahara and Arabian deserts,

369   the mean updraft velocity is ~0.5 m s^{-1}. However, downwind of the western part of the

370   Sahara the aerosol number concentration is relatively low (~1,000 cm^{-3}) leading to

371   higher s_{max} (~0.2%) but low CDNC (~200 cm^{-3}). On the other hand, downwind of the

372   eastern Sahara and Arabian deserts the aerosol concentration is higher (2,000-3,000

373   cm^{-3}). Over these areas the presence of a high number of coarse dust particles

374   significantly reduces s_{max} (~0.05%), but at the same time they efficiently activate into

375   cloud droplets (CDNC varies from 500 to 1,000 cm^{-3}). Close to Patagonia and

376   Australia, despite the high updraft velocities (~1 m s^{-1}), the aerosol concentration is

377   low (below 500 cm^{-3}) and also CDNC is relatively low (~100 cm^{-3}). The highest

378   updraft velocities are calculated around the Atacama and Gobi deserts (over 1 m s^{-1})

379   leading to both high s_{max} (over 0.3%) and CDNC (~1,000 cm^{-3}). However, the central

380   Asian deserts (e.g., Gobi) are under the influence of the Siberian anticyclone during

381   winter (i.e., DJF) which causes katabatic winds (that inhibit the formation of positive

382   updraft velocities) and very low temperatures that prevent the formation of liquid

383   clouds.

384   Over the oceans, the predicted annual mean CDNC is 113 cm^{-3} and exceeds 500

385   cm^{-3} along the coasts of Mediterranean countries, China, India, SE Asia, California,

386   the northeastern USA and western Africa (Fig. 1). Over many coastal regions aerosol

387   concentrations are relatively high (5,000-10,000 cm^{-3}), however, the low updraft

388   velocities (~0.2 m s^{-1}) result in lower CDNCs than over land (Figure 1). The

389   Mediterranean and Yellow Seas are somewhat exceptional since the annual mean

390   updraft velocities are higher (~0.3 m s^{-1}), resulting in higher s_{max} (~0.1% and ~0.3%,

391   respectively) and therefore high CDNC (~800 cm^{-3} and ~1200 cm^{-3}, respectively).

392   The simulated s_{max} is in close agreement with estimates (~0.1%) based on

393   observational data over the eastern Mediterranean (Bougiatioti et al., 2016a;

394   Kalkavouras et al., 2016). CDNC over these seas is subject to high seasonal variation

395   ranging from ~400 cm^{-3} (~800 cm^{-3}) over the Mediterranean (Yellow) Sea during JJA,

396   to over 1,000 cm^{-3} (2,000 cm^{-3}) during DJF due to the higher updraft velocities during

397   boreal winter (exceeding 1 m s^{-1}) compared to summer (below 0.2 m s^{-1}). Over the

398   northern coasts, the annual mean CDNC is significantly enhanced compared to the

399   oceans of the Southern Hemisphere due to the transport of pollutants from

400   industrialized areas in the Northern Hemisphere. Despite the high updraft velocities

401   calculated over the southern oceans throughout the year (up to 1 m s^{-1}), the lack of

402   aerosol (typically below 100 cm^{-3}) results in CDNC below 50 cm^{-3}. Finally, the

403   calculated CDNC decreases with altitude due to the decrease in aerosol concentration

404   by dilution and atmospheric removal (Figure 3). The global mean CDNC is predicted

405   to be 231 cm^{-3}, 171 cm^{-3}, 120 cm^{-3}, 87 cm^{-3}, and 60 cm^{-3} at 940 mb, 900 mb, 860 mb,

406   820 mb, and 770 mb, respectively.

407

408   **3.2   Model Evaluation**

409   The predicted CDNC are compared to observational data from continental,

410   polluted marine and clean marine regions around the world (Karydis et al., 2011). The

411   locations of observations (i.e., longitude, latitude, and altitude) and time of year have

412   been taken into account in sampling the model results. Given that the observations

413   span a decade, in contrast to the simulation which represents one year, the month of

414   each campaign has been used to account for the seasonal variability of the CDNC.

415   Thus, the implicit assumption is that inter-annual variability can be neglected. It

416   should also be mentioned that the observations typically do not represent monthly

417   means over 1.9° grid squares, as sampled from the model results, so that the

418   comparison is more qualitative than quantitative. A summary of the comparison

419   results is presented in Table 1 and Figure 4. The mean bias (MB), mean absolute

420   gross error (MAGE), normalized mean bias (NMB), normalized mean error (NME),

421   and the root mean square error (RMSE) are used to assess the model performance

422   (Table 2).

Atmospheric
Chemistry
and Physics
Discussions

423   The model captures the low values (below 100 cm^{-3}) observed over the remote

424   Pacific, Atlantic and Indian Oceans and at the same time is capable of simulating the

425   higher concentrations (>100 cm^{-3}) observed over the eastern Pacific Ocean (Table 1).

426   On the other hand, it falls short in reproducing the relatively high CDNC (>100 cm^{-3})

427   observed during summer over the western Arctic Ocean and over the remote area west

428   of Australia. Overall, the model tends to underestimate the CDNC over remote oceans

429   with a MB = -33 cm^{-3} and NMB = -39% (Table 2).

430   Both the observed and simulated CDNC show significant increases over polluted

431   marine regions close to the coasts (Table 1; Figure 4a). Compared to satellite

432   retrievals (Bennartz, 2007; Rausch et al., 2010), the model reproduces the CDNC over

433   the American and African coasts well, but it significantly overestimates CDNC along

434   the Asian coasts (Table 1). Compared to in situ observations, the model reproduces

435   the high CDNC along coastal areas in the Northern Hemisphere (e.g., the Yellow Sea,

436   Oregon, Florida, Canary Islands), but systematically overestimates CDNC over the

437   British coasts. Further, the model does not reproduce some of the high CDNC

438   observations over more remote areas (i.e, over the Azores and eastern Atlantic

439   Ocean). Overall, the model tends to overestimate the CDNC over polluted marine

440   areas with a MB = 127 cm^{-3} and NMB = 75% (Table 2).

441   The observed CDNC over continental regions is subject to high variability, with

442   reported values ranging from <100 cm^{-3} over Alaska (Dong and Mace, 2003) to

443   >1,000 cm^{-3} over China (Zhao et al., 2006), England (Bower et al., 1999), and the

444   continental USA (Fountoukis et al., 2007). The model captures the observed

445   variability with low values over remote areas (e.g., over Alaska) and high values over

446   the industrialized parts of the Northern Hemisphere (i.e., East Asia, Europe, and

447   China). Overall, the model overestimates CDNC over most regions (MB= 269 cm^{-3}

448   and NMB=58%; Table 2). Over China, the simulated CDNC is within the observed

449   range with the exception of Hebei Province where it significantly overestimates

450   measured CDNC (Table 1). In Europe, the model reproduces the high CDNC

451   observed over Central Europe and England but it clearly overestimates the low CDNC

452   values observed over Finland. Over North America, the model captures the variability

453   of the observed CDNC, predicting lower values over remote areas (e.g., Alaska) and

454   higher values over the industrialized areas of USA (e.g., Ohio and Michigan). It tends

455   to overestimate the CDNC over the continental USA and underestimate the observed

456   values over Alaska.

Atmospheric
Chemistry
and Physics
Discussions

457   Over all examined regions (clean marine, polluted marine, continental), the

458   calculated NMB is 56% and the NME is 82%, indicating that some of the discrepancy

459   between the modelled and the observed CDNC is explained by uncertainties in the

460   observations and the numerical simulations. Around 60% of the simulated CDNC are

461   within a factor of 2 compared to the measurements (Figure 4a) and 40% of the

462   simulated CDNC differ less than 30% from the measurements. Based on the typical

463   properties of marine stratus clouds, a uniform increase in global CDNC by 30% (or

464   50%) can result in a perturbation of -1.1 W m^{-2} (or -1.7 W m^{-2}) in the global mean

465   cloud radiative forcing (Schwartz, 1996). However, the simulated CDNC presented

466   here refers to the number concentration of droplets nucleated in clouds and represents

467   an upper limit with respect to the comparison with observations, since collision and

468   coalescence processes, which are not taken into account here, can reduce the CDNC.

469

470   **4. Mineral Dust Effect on CDNC**

471

472   **4.1 Total Impact of Mineral Dust on CDNC**

473   To estimate the overall effect of mineral dust on CDNC a sensitivity run was

474   conducted switching off the mineral dust emissions. Figure 5 depicts the difference in

475   CDNC between the base case simulation and the sensitivity test. A positive change

476   corresponds to an increase of the CDNC due to the presence of dust. The predicted

477   CDNC is typically increased by the presence of dust aerosols over the main deserts

478   (Figure 5). Over the Sahara, CDNC increases less than 50 cm^{-3} (up to 20%). The

479   largest change is calculated downwind of the Patagonian (~150 cm^{-3} or 70%) and

480   Atacama (~350 cm^{-3} or 40%) deserts. Over these deserts dust emissions increase the

481   aerosol concentration by more than 5,000 cm^{-3}. The effect of mineral dust on CDNC

482   close to Sahara varies significantly throughout the year due to the seasonality of the

483   mineral dust emissions. Over the sub-Sahelian region, CDNC increases by up to 150

484   cm^{-3} during DJF, owing to the northeasterly trade winds (i.e., Harmattan winds) which

485   blow from the Sahara Desert over the West Africa during winter. Over the eastern

486   Sahara and the Arabian deserts CDNC increase up to 150 cm^{-3} during spring (i.e.,

487   MAM) and autumn (i.e, SON) when the Sirocco winds are most common. In contrast

488   to regions close to deserts, CDNC decreases over the polluted regions of the Northern

489   Hemisphere and especially over southern Europe (~100 or less than 10%) and

490   northeastern Asia (up to 400 cm^{-3} or 20%). In these areas, dust particles transported

Atmospheric
Chemistry
and Physics
Discussions

491 from the Sahara over Europe and from the Gobi and Taklimakan deserts over Asia,

492 are mixed with anthropogenic particles affecting the aerosol-water vapor interactions.

493 As the insoluble fraction of aerosols increases, the exponent x in Eq. 4 changes,

494 resulting in a decrease of the number of activated droplets. Furthermore, the relatively

495 large, aged dust particles over these areas activate early on in the cloud formation

496 process, taking up much water per particle and thus reducing s_{max} (~15%), and

497 consequently cloud droplet formation on the smaller anthropogenic particles (e.g., the

498 activated fraction of the particles in the accumulation mode reduces by 20%). Beside

499 microphysical effects, the presence of mineral dust can also affect cloud formation by

500 altering the energy balance of the atmosphere, and thus turbulent motions and the

501 updraft velocity. Nevertheless, the calculated updraft velocity does not change

502 significantly between the two simulations (less than 5%) since the meteorology is

503 dynamically nudged to analysis data (Jeuken et al., 1996). CDNC also decreases over

504 the oceans downwind of deserts in the Northern Hemisphere, and even over the

505 rainforests in the Southern Hemisphere (~150 or 30%). Overall, despite that CDNC

506 increases over the deserts due to the presence of dust particles, the decrease of CDNC

507 over the industrialized and forested continental areas dominates the calculated global

508 average change, i.e., the calculated global average CDNC decreases by 11% (or 26

509 cm^{-3}).

510

511 **4.2 Impact of Mineral Dust Chemistry on CDNC**

512 To estimate the effects of thermodynamic mineral dust interactions with inorganic

513 anions on the predicted CDNC, a sensitivity run was conducted by switching off the

514 dust-aerosol chemistry. Karydis et al. (2016) have shown that dust can significantly

515 affect the partitioning of inorganic aerosol components and especially nitrate.

516 Analogous to (Karydis et al. (2016)), accounting for thermodynamic interactions of

517 mineral dust in our simulations results in an increase of the tropospheric burden of

518 nitrate, chloride, and sulfate aerosols by 44%, 9%, and 7%, respectively. On the other

519 hand, ammonium decreases by 41%. The dust presence itself also decreases by 14%

520 since it becomes significantly more soluble, mostly due to the condensation of nitric

521 acid on its surface, and is removed more efficiently through wet and dry deposition,

522 the latter due to the increased sedimentation by dust particles that have a larger water

523 content. Therefore, the calculated change of CDNC (Figures 6a and 6b) is the net

Atmospheric
Chemistry
and Physics
Discussions

524   result of counterbalancing effects. Due to the increase of the soluble fraction by

525   considering mineral dust chemistry, the CDNC activated from dust particles increases

526   (Figure 6c), while the total number of dust particles and the CDNC from insoluble

527   particles decreases (Figure 6d). Taking as an example a grid cell over the Sahara

528   desert, the model simulations indicate that by switching on the mineral dust

529   chemistry, the soluble fraction of the dust containing particles increases by 0.07,

530   resulting in an increase of CDNC activated from soluble aerosol modes by 150 cm^{-3}

531   (Figure 6c). On the other hand, the aerosol number concentration decreases by 90 cm^{-3}

532   due to the more efficient atmospheric removal of the aged dust particles, resulting in

533   a decrease of the CDNC activated from the insoluble modes by 50 cm^{-3} (Figure 6d).

534   The net effect is that the total CDNC increases by 100 cm^{-3} (Figure 6a).

535   Overall, the presence of reactive dust components results in an increase of CDNC

536   over the deserts that are close to anthropogenic sources, e.g., up to 100 cm^{-3} (or 20%)

537   over the Sahara and up to 200 cm^{-3} (or 30%) over the Arabian Peninsula. In these

538   areas, the CCN activity of mineral dust (initially hydrophilic) is enhanced by the

539   acquired hygroscopicity from the anthropogenic (including biomass burning) aerosol

540   compounds (mainly nitrate) during their thermodynamic interaction. Even though the

541   chemically aged dust particles activate into droplets more efficiently than insoluble

542   ones, their reduced number concentration dominates the calculated effect on CDNC

543   over the relatively pristine remote desert regions, e.g., CDNC decreases up to 200 cm^{-3}

544   (or 20%) downwind of the Taklimakan, 250 cm^{-3} (or 30%) around the Atacama, and

545   up to 100 cm^{-3} (or 40%) over the Patagonian deserts. Even over the rainforests, HNO_3

546   from biomass burning NO_X thermodynamically interacts with the coarse soil particles

547   from the upwind deserts, resulting in an increase of CDNC by around 50 cm^{-3}. CDNC

548   is also slightly increased over Europe and eastern Asia (up to 150 cm^{-3} or about 10%)

549   where HNO_3 from anthropogenic NO_X sources interacts with mineral dust from the

550   surrounding deserts. While the global average CDNC does not change much by taking

551   into account thermodynamic and chemical interactions of mineral dust with inorganic

552   air pollutants, CDNC spatial distributions change substantially.

553

554   **4.3 Impact of Water Adsorption by Mineral Dust on CDNC**

555   To estimate the effects of water adsorption onto the surface of insoluble dust

556   particles on CDNC, a sensitivity run was conducted by switching off the FHH

557   adsorption calculations. In this sensitivity simulation, the soluble modes follow the κ-

Atmospheric
Chemistry
and Physics
Discussions

558   Köhler theory while insoluble modes do not participate in cloud droplet formation

559   calculations. Figure 7 depicts the difference in CDNC between the base case

560   simulation and this sensitivity test. A positive change corresponds to an increase of

561   the CDNC from water adsorption on mineral dust. The calculations show that CDNC

562   is increased by applying FHH theory over several arid areas where the insoluble dust

563   concentration is high (Figure 7), since κ-Köhler theory does not take into account the

564   contribution of insoluble particles to cloud droplet formation. CDNC is increased in

565   the vicinity of the Sahara, Arabian and Thar deserts (~100 cm^{-3} or about 20%) where

566   the insoluble fraction of mineral dust is larger due to the small anthropogenic

567   emission influence that makes the particles hygroscopic. On the other hand, CDNC

568   decreases over the polluted regions of the Northern Hemisphere and especially over

569   Europe (~100 cm^{-3} or about 10%) and Asia (up to 400 cm^{-3} or ~20%). Over these

570   areas, the added hydrophilicity by the soluble coatings on the surface of the aged dust

571   particles increases their water uptake during activation. Therefore, the aged dust

572   particles relatively strongly compete for water vapor, reducing the s_{max} (~15%) and

573   thus cloud droplet formation from the smaller anthropogenic particles. Over the

574   tropical rainforests CDNC decreases by approximately 150 cm^{-3} (or ~30%). Overall,

575   the use of the UAF results in a decrease of the global average CDNC by ~10% (or

576   about 23 cm^{-3}).

577

578   **5   Additional Sensitivity Tests**

579   Three additional sensitivity simulations were conducted to investigate the CDNC

580   dependency on i) the chemical composition of the emitted dust aerosols, ii) the

581   hydrophilicity of mineral dust, and iii) the strength of the dust aerosol emissions.

582   Figure 8 depicts the absolute annual mean changes in CDNC compared to the

583   reference simulation for each of the sensitivity tests. A positive change corresponds to

584   an increase of the CDNC relative to the reference.

585

586   **5.1 Sensitivity to the emitted dust aerosol composition**

587   The first sensitivity test assumes a globally uniform chemical composition of

588   mineral dust (Sposito, 1989), in contrast to the reference simulation where the mineral

589   dust composition depends on the soil characteristics of each desert (Karydis et al.,

590   2016). While the emitted mineral dust load remains the same in the sensitivity

591   simulation, the different mineral dust composition results in significant changes in the

592   calculated tropospheric burdens of dust components (Karydis et al., 2016). In

593   particular, the fraction of the mineral components relative to the total dust in the

594   sensitivity simulation is lower over most of the deserts compared to the reference.

595   This reduction of the chemically reactive mineral components in the sensitivity

596   simulation results in a slowdown of the mineral dust aging and hence in an increase of

597   its concentration due to the reduced atmospheric removal. Conversely, the CCN

598   activity of dust particles is higher in the reference simulation since the chemical aging

599   is stronger compared to the sensitivity simulation. These counterbalancing effects

600   result in negligible changes of CDNC worldwide (less than 10%).

601

602

603

604   **5.2 Sensitivity to the hydrophilicity of dust**

605   The second sensitivity test assumes increased hydrophilicity of mineral dust

606   aerosols by using a 10% lower B_{FHH} parameter (B_{FHH}=1.1). The higher hydrophilicity

607   of mineral dust in the sensitivity simulation results in increased CDNC over over

608   areas close to deserts by up to 30% (e.g., 100 cm^{-3} over Sahara and 200 cm^{-3} over

609   Gobi and Taklimakan). A notable increase is also calculated over eastern China and

610   northern India (up to 150 cm^{-3} or 10%) where mineral dust is mixed with

611   anthropogenic compounds. Remote from the main deserts (e.g., over central Europe),

612   the change in CDNC is negligible since the contribution of mineral dust particles on

613   cloud droplet formation is low. Overall, the calculated global average CDNC

614   increases in the sensitivity simulation by 5% (or 12 cm^{-3}).

615

616   **5.3 Sensitivity to the emitted dust aerosol load**

617   The final sensitivity test assumes 50% lower emissions of mineral dust compared

618   to the reference simulation. The lower tropospheric dust aerosol load in the sensitivity

619   simulation (49%) results in a 10-30% (up to 150 cm^{-3}) decrease of CDNC over the

620   main deserts. On the other hand, CDNC increases over the anthropogenic (e.g., East

621   Asia) and biomass burning (e.g., central Africa) regions by 5-10% (up to 150 cm^{-3}).

622   The opposing responses of CDNC to mineral dust emissions result from the fact that

623   the tropospheric load of the other aerosol species does not change significantly

624   between the two simulations since the chemical and thermodynamic interactions of

Atmospheric
Chemistry
and Physics
Discussions

625 mineral cations with air pollution are still important even after the 50% emission

626 reduction of dust. Therefore, the presence of inorganic anions (e.g., NO_3^-) in the

627 aerosol phase remains almost unchanged between the two simulations which results in

628 a decrease of the insoluble fraction of the aerosol, given that mineral dust

629 concentrations are significantly lower in the reference simulation, leading to higher

630 CCN activity. Over the Taklimakan desert the insoluble fraction of the aerosol

631 changes by less than 10%, and therefore, the change in aerosol number concentration

632 (~40%) due to the mineral dust emission change dominates the effect on CDNC,

633 which is calculated to be about 100 cm^{-3} (or ~20%) lower in the sensitivity

634 simulation. On the other hand, over Southeast Asia, the aerosol number concentration

635 changes less than 10% while the insoluble fraction of the aerosols decreases by 40%.

636 The significant decrease of ε_i in Eq. (3) affects the calculated critical supersaturation

637 of the particle as well as the exponent x in Eq. (4) resulting in an increase of CDNC

638 by about 150 cm^{-3} (or ~10%). Overall, the impact of halving mineral dust emissions

639 on the calculated global average CDNC is remarkably small (~3% or 6 cm^{-3}).

640
641

642 **6   Summary and Conclusions**

643   This study assesses the impact of mineral dust on global cloud droplet number

644 concentrations by using an interactive aerosol-chemistry-cloud-climate model

645 (EMAC). The "unified dust activation framework" (UAF) has been implemented into

646 the EMAC model to account for the effects of dust particles through both the

647 hydrophilicity from adsorption and the acquired hygroscopicity from pollution solutes

648 (chemical aging) on CCN activity calculations. The calculation of cloud droplet

649 formation from soluble particles is carried out by using the κ-Köhler theory, while

650 that of insoluble particles is based on the FHH multilayer adsorption isotherm

651 approach. For atmospheric particles that contain a substantial fraction of both soluble

652 (e.g., nitrate) and insoluble material (e.g., mineral dust), cloud formation is calculated

653 using the UAF, which determines the maximum equilibrium water vapor

654 supersaturation over an aerosol consisting of an insoluble core with a soluble coating.

655 Furthermore, the model setup includes thermodynamic interactions between mineral

656 dust anions (i.e., Na^+, Ca^{2+}, K^+, Mg^{2+}) and inorganic cations (i.e., NO_3^-, Cl^-, SO_4^{2-}).

657   The simulated CDNC at 940 mb, i.e., at cloud base, is relatively high over the

658 industrialized areas of Europe, Asia and North America (exceeding 1,000 cm^{-3}) and

Atmospheric
Chemistry
and Physics
Discussions

Open Access

659 over the biomass burning regions in the tropics (300-700 cm^{-3}). Relatively high

660 CDNC is also calculated over the main deserts (100-1,000 cm^{-3}) where the CCN

661 activity of pristine mineral dust is enhanced by chemical and thermodynamic

662 interactions with soluble compounds from anthropogenic (including biomass burning)

663 and natural sources. Low CDNC (around 50 cm^{-3}) is calculated over the remote

664 oceans while CDNC is much higher (up to 1,000 cm^{-3}) over more polluted marine

665 regions near the coast. In view of CDNCs from in situ and satellite observations, we

666 conclude that the model tends to underestimate CDNC over clean marine areas and

667 overestimates CDNC over polluted regions.

668 To estimate the effects of mineral dust and its variable chemical composition on

669 CDNC, three main sensitivity simulations have been conducted. In the first, mineral

670 dust emissions were switched off. This reveals that despite the large tropospheric load

671 of mineral dust aerosols (35 Tg in the base case simulation) the dust presence

672 decreases the calculated global average CDNC by only 11%. This is the net result of

673 substantial positive and negative, partly compensating effects. Over polluted regions

674 (e.g., Europe), dust particles, mostly transported from the Sahara, are mixed with

675 pollution aerosols resulting in a significant reduction of the CCN activity of the

676 anthropogenic particles and hence cloud droplet formation. On the other hand, the

677 activation of freshly emitted dust particles through water adsorption results in an

678 increase of CDNC over the main deserts. However, on a global scale this does not

679 match the calculated decrease over the polluted regions. While such sensitivity tests

680 do not relate to real-world changes, they help understand the role of mineral dust in

681 the climate system, and especially the importance of including these processes into

682 climate models, being hitherto neglected.

683 A second simulation has been performed by switching off the mineral dust

684 chemistry to estimate the impact of interactions between inorganic and mineral

685 cations on the predicted CDNC. We find that the tropospheric burden of inorganic

686 anions (mainly nitrate) increases, resulting in a slight increase of CCN activity and

687 cloud droplet formation in areas that are influenced by biomass burning and industrial

688 emissions. Furthermore, including crustal cation chemistry and thermodynamics

689 significantly affects the aging of mineral dust and its solubility, especially due to the

690 uptake of nitric acid, so that dust is removed more efficiently through wet and dry

691 deposition. This results in a decrease of CDNC over the remote deserts (e.g.,

Atmospheric
Chemistry
and Physics
Discussions

692   Taklimakan). On average, global CDNC does not change significantly by considering

693   mineral dust chemistry and thermodynamics.

694   In the third simulation the FHH calculations have been switched off to estimate the

695   effects of water adsorption onto the surface of insoluble dust particles on the predicted

696   CDNC. The CDNC in the reference simulation is found to be higher over arid areas

697   due to the adsorption activation of the freshly emitted insoluble dust particles. On the

698   other hand, CDNC is lower over polluted regions (e.g., over Europe) since the aged

699   dust particles experience significant water uptake during their activation reducing the

700   s_{max} and the activation of the smaller anthropogenic particles. Overall, the use of the

701   UAF results in a decrease of the global average CDNC by ~10%. This result shows

702   that for the modeling of cloud droplet formation, adsorption activation of insoluble

703   aerosols is more important than mineral dust chemistry and thermodynamics.

704   However, taking into account the adsorption activation of insoluble aerosols without

705   mineral dust chemistry can result in a significant overestimation of CDNC, mainly

706   over the remote deserts. Conversely, considering mineral dust chemistry and

707   thermodynamics without UAF can result in significant overestimation of CDNC over

708   polluted areas.

709   Finally, three additional sensitivity simulations have been conducted to investigate

710   the sensitivity of the results to the physicochemical properties of the emitted mineral

711   dust (chemical composition, hydrophilicity and emission strength). This indicates that

712   the calculated CDNC is sensitive to the mineral dust hydrophilicity and emission load.

713   By assuming drastic differences in the dust source and the dust hydrophilicity, we find

714   only small (~5%) changes in the average CDNC. Further, the global average CDNC is

715   not sensitive to the chemical composition of mineral dust.

716   This study demonstrates that a comprehensive treatment of the CCN activity of

717   mineral dust aerosols and their chemical and thermodynamic interactions with

718   inorganic species by CCMs is important to realistically account for aerosol-chemistry-

719   cloud-climate interactions. Neglecting the adsorption activation of freshly emitted

720   dust can result in significant biases over areas close to deserts. In addition, neglecting

721   the mineral dust chemistry and thermodynamics results in an underestimation of the

722   coating of dust by hygroscopic salts during atmospheric aging. The realistic

723   representation of soluble coating on dust is crucial since it affects its efficiency to

724   grow by water uptake, which significantly influences the local supersaturation and

Atmospheric
Chemistry
and Physics
Discussions

725   thus cloud droplet formation over anthropogenically polluted regions. In this first

726   study we apply the UAF diagnostically, while for future applications, e.g., to simulate

727   climate effects, we plan prognostic climate calculations where effects on precipitation

728   formation and dynamical responses will also be accounted for.

729

734

735

References

736 **References**

737

738 Abdelkader, M., Metzger, S., Mamouri, R. E., Astitha, M., Barrie, L., Levin, Z., and Lelieveld, J.:
739   Dust-air pollution dynamics over the eastern Mediterranean, Atmospheric Chemistry and Physics,
740   15, 9173-9189, 2015.
741 Albrecht, B. A.: Aerosols, cloud microphysics, and fractional cloudiness, Science, 245, 1227-1230,
742   1989.
743 Andreae, M. O. and Rosenfeld, D.: Aerosol-cloud-precipitation interactions. Part 1. The nature and
744   sources of cloud-active aerosols, Earth-Science Reviews, 89, 13-41, 2008.
745 Astitha, M., Lelieveld, J., Kader, M. A., Pozzer, A., and de Meij, A.: Parameterization of dust
746   emissions in the global atmospheric chemistry-climate model EMAC: impact of nudging and soil
747   properties, Atmospheric Chemistry and Physics, 12, 11057-11083, 2012.
748 Bangert, M., Nenes, A., Vogel, B., Vogel, H., Barahona, D., Karydis, V. A., Kumar, P., Kottmeier, C.,
749   and Blahak, U.: Saharan dust event impacts on cloud formation and radiation over Western Europe,
750   Atmospheric Chemistry and Physics, 12, 4045-4063, 2012.
751 Barahona, D. and Nenes, A.: Parameterization of cloud droplet formation in large-scale models:
752   Including effects of entrainment, J. Geophys. Res., 112, doi:10.1029/2007JD008473 2007.
753 Barahona, D., West, R. E. L., Stier, P., Romakkaniemi, S., Kokkola, H., and Nenes, A.:
754   Comprehensively accounting for the effect of giant CCN in cloud activation parameterizations,
755   Atmos. Chem. Phys., 10, 2467-2473, 2010.
756 Begue, N., Tulet, P., Pelon, J., Aouizerats, B., Berger, A., and Schwarzenboeck, A.: Aerosol processing
757   and CCN formation of an intense Saharan dust plume during the EUCAARI 2008 campaign,
758   Atmospheric Chemistry and Physics, 15, 3497-3516, 2015.
759 Bennartz, R.: Global assessment of marine boundary layer cloud droplet number concentration from
760   satellite, J. Geophys. Res., 112, doi: 10.1029/2006JD007547 2007.
761 Betancourt, R. M. and Nenes, A.: Droplet activation parameterization: the population-splitting concept
762   revisited, Geoscientific Model Development, 7, 2345-2357, 2014a.
763 Betancourt, R. M. and Nenes, A.: Understanding the contributions of aerosol properties and
764   parameterization discrepancies to droplet number variability in a global climate model,
765   Atmospheric Chemistry and Physics, 14, 4809-4826, 2014b.
766 Bougiatioti, A., Bezantakos, S., Stavroulas, I., Kalivitis, N., Kokkalis, P., Biskos, G., Mihalopoulos, N.,
767   Papayannis, A., and Nenes, A.: Biomass-burning impact on CCN number, hygroscopicity and cloud
768   formation during summertime in the eastern Mediterranean, Atmospheric Chemistry and Physics,
769   16, 7389-7409, 2016a.
770 Bougiatioti, A., Nikolaou, P., Stavroulas, I., Kouvarakis, G., Weber, R., Nenes, A., Kanakidou, M., and
771   Mihalopoulos, N.: Particle water and pH in the eastern Mediterranean: source variability and
772   implications for nutrient availability, Atmospheric Chemistry and Physics, 16, 4579-4591, 2016b.
773 Bouwman, A. F., Lee, D. S., Asman, W. A. H., Dentener, F. J., VanderHoek, K. W., and Olivier, J. G.
774   J.: A global high-resolution emission inventory for ammonia, Global Biogeochemical Cycles, 11,
775   561-587, 1997.
776 Bower, K. N., Choularton, T. W., Gallagher, M. W., Colvile, R. N., Beswick, K. M., Inglis, D. W. F.,
777   Bradbury, C., Martinsson, B. G., Swietlicki, E., Berg, O. H., Cederfelt, S. I., Frank, G., Zhou, J.,
778   Cape, J. N., Sutton, M. A., McFadyen, G. G., Milford, C., Birmili, W., Yuskiewicz, B. A.,
779   Wiedensohler, A., Stratmann, F., Wendisch, M., Berner, A., Ctyroky, P., Galambos, Z., Mesfin, S.
780   H., Dusek, U., Dore, C. J., Lee, D. S., Pepler, S. A., Bizjak, M., and Divjak, B.: The Great Dun Fell
781   Experiment 1995: an overview, Atmospheric Research, 50, 151-184, 1999.
782 Capps, S. L., Henze, D. K., Hakami, A., Russell, A. G., and Nenes, A.: ANISORROPIA: the adjoint of
783   the aerosol thermodynamic model ISORROPIA, Atmospheric Chemistry and Physics, 12, 527-543,
784   2012.
785 Clarke, L., Edmonds, J., Jacoby, H., Pitcher, H., Reilly, J., and Richels, R.: Scenarios of greenhouse
786   gas emissions and atmospheric concentrations (Part A) and review of integrated scenario
787   development and application (Part B). A report by the U.S. climate change science program and the
788   subcommittee on global change research, 2007. 2007.
789 Considine, D. B., Bergmann, D. J., and Liu, H.: Sensitivity of Global Modeling Initiative chemistry and
790   transport model simulations of radon-222 and lead-210 to input meteorological data, Atmospheric
791   Chemistry and Physics, 5, 3389-3406, 2005.
792 Dall'Osto, M., Harrison, R. M., Highwood, E. J., O'Dowd, C., Ceburnis, D., Querol, X., and
793   Achterberg, E. P.: Variation of the mixing state of Saharan dust particles with atmospheric
794   transport, Atmospheric Environment, 44, 3135-3146, 2010.

795 de Meij, A., Pozzer, A., Pringle, K. J., Tost, H., and Lelieveld, J.: EMAC model evaluation and
796   analysis of atmospheric aerosol properties and distribution with a focus on the Mediterranean
797   region, Atmos. Res., 114, 38-69, 2012.
798 Dentener, F., Kinne, S., Bond, T., Boucher, O., Cofala, J., Generoso, S., Ginoux, P., Gong, S.,
799   Hoelzemann, J. J., Ito, A., Marelli, L., Penner, J. E., Putaud, J. P., Textor, C., Schulz, M., van der
800   Werf, G. R., and Wilson, J.: Emissions of primary aerosol and precursor gases in the years 2000
801   and 1750 prescribed data-sets for AeroCom, Atmos. Chem. Phys., 6, 4321-4344, 2006.
802 Doering, U., van Aardenne, J., Monni, S., Pagliari, V., Orlandini, L., and SanMartin, F.: CIRCE report
803   D8.1.3 – Update of gridded emission inventories, addition of period 1990–2005 and the years 2010,
804   2015, 2050, 036961, 2009.
805 Dong, X. Q. and Mace, G. G.: Arctic stratus cloud properties and radiative forcing derived from
806   ground-based data collected at Barrow, Alaska, Journal of Climate, 16, 445-461, 2003.
807 Drozd, G., Woo, J., Häkkinen, S. A. K., Nenes, A., and McNeill, V. F.: Inorganic salts interact with
808   oxalic acid in submicron particles to form material with low hygroscopicity and volatility, Atmos.
809   Chem. Phys., 14, 5205-5215, 2014.
810 Fairlie, T. D., Jacob, D. J., Dibb, J. E., Alexander, B., Avery, M. A., van Donkelaar, A., and Zhang, L.:
811   Impact of mineral dust on nitrate, sulfate, and ozone in transpacific Asian pollution plumes,
812   Atmospheric Chemistry and Physics, 10, 3999-4012, 2010.
813 Falkovich, A. H., Ganor, E., Levin, Z., Formenti, P., and Rudich, Y.: Chemical and mineralogical
814   analysis of individual mineral dust particles, Journal of Geophysical Research-Atmospheres, 106,
815   18029-18036, 2001.
816 Feingold, G., Cotton, W. R., Kreidenweis, S. M., and Davis, J. T.: The impact of giant cloud
817   condensation nuclei on drizzle formation in stratocumulus: Implications for cloud radiative
818   properties, Journal of the Atmospheric Sciences, 56, 4100-4117, 1999.
819 Feng, Y. and Penner, J. E.: Global modeling of nitrate and ammonium: Interaction of aerosols and
820   tropospheric chemistry, Journal of Geophysical Research-Atmospheres, 112, 2007.
821 Fountoukis, C. and Nenes, A.: Continued development of a cloud droplet formation parameterization
822   for global climate models, J. Geophys. Res., 110, doi: 10.1029/2004JD005591, 2005.
823 Fountoukis, C. and Nenes, A.: ISORROPIA II: a computationally efficient thermodynamic equilibrium
824   model for K^+-Ca^{2+}-Mg^{2+}-NH_4^+-Na^+-SO_4^{2-}-NO_3^--Cl^--H_2O aerosols, Atmospheric Chemistry and
825   Physics, 7, 4639-4659, 2007.
826 Fountoukis, C., Nenes, A., Meskhidze, N., Bahreini, R., Conant, W. C., Jonsson, H., Murphy, S.,
827   Sorooshian, A., Varutbangkul, V., Brechtel, F., Flagan, R. C., and Seinfeld, J. H.: Aerosol-cloud
828   drop concentration closure for clouds sampled during the International Consortium for Atmospheric
829   Research on Transport and Transformation 2004 campaign, J. Geophys. Res., 112, doi:
830   10.1029/2006JD007272, 2007.
831 Fountoukis, C., Nenes, A., Sullivan, A., Weber, R., Van Reken, T., Fischer, M., Matias, E., Moya, M.,
832   Farmer, D., and Cohen, R. C.: Thermodynamic characterization of Mexico City aerosol during
833   MILAGRO 2006, Atmospheric Chemistry and Physics, 9, 2141-2156, 2009.
834 Gantt, B., He, J., Zhang, X., Zhang, Y., and Nenes, A.: Incorporation of advanced aerosol activation
835   treatments into CESM/CAM5: model evaluation and impacts on aerosol indirect effects,
836   Atmospheric Chemistry and Physics, 14, 7485-7497, 2014.
837 Ganzeveld, L. N., Lelieveld, J., Dentener, F. J., Krol, M. C., Bouwman, A. J., and Roelofs, G. J.:
838   Global soil-biogenic NOx emissions and the role of canopy processes, Journal of Geophysical
839   Research-Atmospheres, 107, 2002.
840 Garimella, S., Huang, Y. W., Seewald, J. S., and Cziczo, D. J.: Cloud condensation nucleus activity
841   comparison of dry- and wet-generated mineral dust aerosol: the significance of soluble material,
842   Atmospheric Chemistry and Physics, 14, 6003-6019, 2014.
843 Giannadaki, D., Pozzer, A., and Lelieveld, J.: Modeled global effects of airborne desert dust on air
844   quality and premature mortality, Atmospheric Chemistry and Physics, 14, 957-968, 2014.
845 Grewe, V., Brunner, D., Dameris, M., Grenfell, J. L., Hein, R., Shindell, D., and Staehelin, J.: Origin
846   and variability of upper tropospheric nitrogen oxides and ozone at northern mid-latitudes,
847   Atmospheric Environment, 35, 3421-3433, 2001.
848 Grini, A., Myhre, G., Zender, C. S., and Isaksen, I. S. A.: Model simulations of dust sources and
849   transport in the global atmosphere: Effects of soil erodibility and wind speed variability, J.
850   Geophys. Res., 110, doi: 10.1029/2004JD005037, 2005.
851 Gustafsson, R. J., Orlov, A., Badger, C. L., Griffiths, P. T., Cox, R. A., and Lambert, R. M.: A
852   comprehensive evaluation of water uptake on atmospherically relevant mineral surfaces: DRIFT
853   spectroscopy, thermogravimetric analysis and aerosol growth measurements, Atmospheric
854   Chemistry and Physics, 5, 3415-3421, 2005.

Atmospheric
Chemistry
and Physics
Discussions

Open Access

EGU

855   Hatch, C. D., Greenaway, A. L., Christie, M. J., and Baltrusaitis, J.: Water adsorption constrained
856   Frenkel-Halsey-Hill adsorption activation theory: Montmorillonite and illite, Atmospheric
857   Environment, 87, 26-33, 2014.
858   Hauglustaine, D. A., Balkanski, Y., and Schulz, M.: A global model simulation of present and future
859   nitrate aerosols and their direct radiative forcing of climate, Atmospheric Chemistry and Physics,
860   14, 11031-11063, 2014.
861   Haywood, J. and Boucher, O.: Estimates of the direct and indirect radiative forcing due to tropospheric
862   aerosols: A review, Reviews of Geophysics, 38, 513-543, 2000.
863   Herich, H., Tritscher, T., Wiacek, A., Gysel, M., Weingartner, E., Lohmann, U., Baltensperger, U., and
864   Cziczo, D. J.: Water uptake of clay and desert dust aerosol particles at sub- and supersaturated
865   water vapor conditions, Phys. Chem. Chem. Phys., 11, 7804-7809, 2009.
866   IPCC: (Intergovernmental Panel on Climate Change): The physical science basis. Contribution of
867   working group I to the fifth assessment report of the intergovernmental panel on climate change.
868   T.F. Stocker, D. Qin, G.-K. Plattner, M. Tignor, S.K. Allen, J. Boschung, A. Nauels, Y. Xia, V.
869   Bex, and P.M. Midgley (eds.). Cambridge University Press, Cambridge, United Kingdom and New
870   York, NY, USA, 2013. 2013.
871   Jeuken, A. B. M., Siegmund, P. C., Heijboer, L. C., Feichter, J., and Bengtsson, L.: On the potential of
872   assimilating meteorological analyses in a global climate model for the purpose of model validation,
873   Journal of Geophysical Research-Atmospheres, 101, 16939-16950, 1996.
874   Jöckel, P., Kerkweg, A., Pozzer, A., Sander, R., Tost, H., Riede, H., Baumgaertner, A., Gromov, S.,
875   and Kern, B.: Development cycle 2 of the Modular Earth Submodel System (MESSy2),
876   Geoscientific Model Development, 3, 717-752, 2010.
877   Jöckel, P., Tost, H., Pozzer, A., Bruehl, C., Buchholz, J., Ganzeveld, L., Hoor, P., Kerkweg, A.,
878   Lawrence, M. G., Sander, R., Steil, B., Stiller, G., Tanarhte, M., Taraborrelli, D., Van Aardenne, J.,
879   and Lelieveld, J.: The atmospheric chemistry general circulation model ECHAM5/MESSy1:
880   consistent simulation of ozone from the surface to the mesosphere, Atmos. Chem. Phys., 6, 5067-
881   5104, 2006.
882   Kalkavouras, P., Bossioli, E., Bezantakos, S., Bougiatioti, A., Kalivitis, N., Stavroulas, I., Kouvarakis,
883   G., Protonotariou, A. P., Dandou, A., Biskos, G., Mihalopoulos, N., Nenes, A., and Tombrou, M.:
884   New Particle Formation in the South Aegean Sea during the Etesians: importance for CCN
885   production and cloud droplet number, Atmos. Chem. Phys. Discuss., 2016, 1-35, 2016.
886   Kallos, G., Solomos, S., Kushta, J., Mitsakou, C., Spyrou, C., Bartsotas, N., and Kalogeri, C.: Natural
887   and anthropogenic aerosols in the Eastern Mediterranean and Middle East: Possible impacts,
888   Science of the Total Environment, 488, 391-399, 2014.
889   Karydis, V. A., Capps, S. L., Russell, A. G., and Nenes, A.: Adjoint sensitivity of global cloud droplet
890   number to aerosol and dynamical parameters, Atmospheric Chemistry and Physics, 12, 9041-9055,
891   2012.
892   Karydis, V. A., Kumar, P., Barahona, D., Sokolik, I. N., and Nenes, A.: On the effect of dust particles
893   on global cloud condensation nuclei and cloud droplet number, Journal of Geophysical Research-
894   Atmospheres, 116, 2011.
895   Karydis, V. A., Tsimpidi, A. P., Pozzer, A., Astitha, M., and Lelieveld, J.: Effects of mineral dust on
896   global atmospheric nitrate concentrations, Atmos. Chem. Phys., 16, 1491-1509, 2016.
897   Kelly, J. T., Chuang, C. C., and Wexler, A. S.: Influence of dust composition on cloud droplet
898   formation, Atmos. Environ., 41, 2904-2916, 2007.
899   Kerkweg, A., Buchholz, J., Ganzeveld, L., Pozzer, A., Tost, H., and Jöckel, P.: Technical Note: An
900   implementation of the dry removal processes DRY DEPosition and SEDImentation in the Modular
901   Earth Submodel System (MESSy), Atmos. Chem. Phys., 6, 4617-4632, 2006.
902   Koch, D., Bauer, S. E., Del Genio, A., Faluvegi, G., McConnell, J. R., Menon, S., Miller, R. L., Rind,
903   D., Ruedy, R., Schmidt, G. A., and Shindell, D.: Coupled Aerosol-Chemistry-Climate Twentieth-
904   Century Transient Model Investigation: Trends in Short-Lived Species and Climate Responses,
905   Journal of Climate, 24, 2693-2714, 2011.
906   Koehler, K. A., Kreidenweis, S. M., DeMott, P. J., Petters, M. D., Prenni, A. J., and Carrico, C. M.:
907   Hygroscopicity and cloud droplet activation of mineral dust aerosol, Geophy. Res. Let., 36, doi:
908   10.1029/2009GL037348, 2009.
909   Kumar, P., Nenes, A., and Sokolik, I. N.: Importance of adsorption for CCN activity and hygroscopic
910   properties of mineral dust aerosol, Geophys. Res. Let., 36, doi: 10.1029/2009GL040827, 2009a.
911   Kumar, P., Sokolik, I. N., and Nenes, A.: Cloud condensation nuclei activity and droplet activation
912   kinetics of wet processed regional dust samples and minerals, Atmos. Chem. Phys., 11, 8661-8676,
913   2011a.

914 Kumar, P., Sokolik, I. N., and Nenes, A.: Measurements of cloud condensation nuclei activity and
915   droplet activation kinetics of fresh unprocessed regional dust samples and minerals, Atmos. Chem.
916   Phys., 11, 3527-3541, 2011b.
917 Kumar, P., Sokolik, I. N., and Nenes, A.: Parameterization of cloud droplet formation for global and
918   regional models: including adsorption activation from insoluble CCN, Atmos. Chem. Phys., 9,
919   2517-2532, 2009b.
920 Kushta, J., Kallos, G., Astitha, M., Solomos, S., Spyrou, C., Mitsakou, C., and Lelieveld, J.: Impact of
921   natural aerosols on atmospheric radiation and consequent feedbacks with the meteorological and
922   photochemical state of the atmosphere, Journal of Geophysical Research-Atmospheres, 119, 1463-
923   1491, 2014.
924 Laaksonen, A., Malila, J., Nenes, A., Hung, H. M., and Chen, J. P.: Surface fractal dimension, water
925   adsorption efficiency, and cloud nucleation activity of insoluble aerosol, Scientific Reports, 6,
926   2016.
927 Lathem, T. L., Kumar, P., Nenes, A., Dufek, J., Sokolik, I. N., Trail, M., and Russell, A.: Hygroscopic
928   properties of volcanic ash, Geophysical Research Letters, 38, 2011.
929 Leibensperger, E. M., Chen, W. T., Seinfeld, J. H., Nenes, A., Adams, P. J., Streets, D. G., Kumar, N.,
930   and Rind, D.: Climatic Effects of 1950-2050 Changes in US Anthropogenic Aerosols - Part 1:
931   Aerosol trends and radiative forcing, Atmo. Chem. Phys., 2011. Submitted, 2011.
932 Lelieveld, J., Evans, J. S., Fnais, M., Giannadaki, D., and Pozzer, A.: The contribution of outdoor air
933   pollution sources to premature mortality on a global scale, Nature, 525, 367-+, 2015.
934 Levin, Z., Teller, A., Ganor, E., and Yin, Y.: On the interactions of mineral dust, sea-salt particles, and
935   clouds: A measurement and modeling study from the Mediterranean Israeli Dust Experiment
936   campaign, J. Geophys. Res., 110, doi: 10.1029/2005JD005810, 2005.
937 Liao, H., Adams, P. J., Chung, S. H., Seinfeld, J. H., Mickley, L. J., and Jacob, D. J.: Interactions
938   between tropospheric chemistry and aerosols in a unified general circulation model, Journal of
939   Geophysical Research-Atmospheres, 108, 2003.
940 Lohmann, U. and Feichter, J.: Global indirect aerosol effects: a review, Atmospheric Chemistry and
941   Physics, 5, 715-737, 2005.
942 Lohmann, U., Feichter, J., Chuang, C. C., and Penner, J. E.: Prediction of the number of cloud droplets
943   in the ECHAM GCM, Journal of Geophysical Research-Atmospheres, 104, 9169-9198, 1999a.
944 Lohmann, U., McFarlane, N., Levkov, L., Abdella, K., and Albers, F.: Comparing different cloud
945   schemes of a single column model by using mesoscale forcing and nudging technique, Journal of
946   Climate, 12, 438-461, 1999b.
947 Ma, J., Chen, Y., Wang, W., Yan, P., Liu, H., Yang, S., Hu, Z., and Lelieveld, J.: Strong air pollution
948   causes widespread haze-clouds over China, Journal of Geophysical Research-Atmospheres, 115,
949   2010.
950 Martin, G. M., Johnson, D. W., and Spice, A.: The measurements and Parameterization of Effective
951   Radius of Droplets in Warm Stratocumulus Clouds, Journal of the Atmospheric Sciences, 51, 1823-
952   1842, 1993.
953 Martin, R. V., Jacob, D. J., Yantosca, R. M., Chin, M., and Ginoux, P.: Global and regional decreases
954   in tropospheric oxidants from photochemical effects of aerosols, Journal of Geophysical Research-
955   Atmospheres, 108, 2003.
956 Morales, R. and Nenes, A.: Characteristic updrafts for computing distribution-averaged cloud droplet
957   number and stratocumulus cloud properties, J. Geophys. Res., 115, doi: 10.1029/2009JD013233,
958   2010.
959 Nenes, A. and Seinfeld, J. H.: Parameterization of cloud droplet formation in global climate models, J.
960   Geophys. Res., 108, doi: 10.1029/2002JD002911, 2003.
961 Perry, K. D., Cliff, S. S., and Jimenez-Cruz, M. P.: Evidence for hygroscopic mineral dust particles
962   from the Intercontinental Transport and Chemical Transformation Experiment, Journal of
963   Geophysical Research-Atmospheres, 109, 2004.
964 Petters, M. D. and Kreidenweis, S. M.: A single parameter representation of hygroscopic growth and
965   cloud condensation nucleus activity, Atmospheric Chemistry and Physics, 7, 1961-1971, 2007.
966 Pozzer, A., de Meij, A., Pringle, K. J., Tost, H., Doering, U. M., van Aardenne, J., and Lelieveld, J.:
967   Distributions and regional budgets of aerosols and their precursors simulated with the EMAC
968   chemistry-climate model, Atmos. Chem. Phys.. 12, 961-987, 2012.
969 Pozzer, A., Jockel, P., and Van Aardenne, J.: The influence of the vertical distribution of emissions on
970   tropospheric chemistry, Atmospheric Chemistry and Physics, 9, 9417-9432, 2009.
971 Pozzer, A., Joeckel, P. J., Sander, R., Williams, J., Ganzeveld, L., and Lelieveld, J.: Technical note: the
972   MESSy-submodel AIRSEA calculating the air-sea exchange of chemical species, Atmos. Chem.
973   Phys., 6, 5435-5444, 2006.

Pringle, K. J., Tost, H., Message, S., Steil, B., Giannadaki, D., Nenes, A., Fountoukis, C., Stier, P., Vignati, E., and Leieved, J.: Description and evaluation of GMXe: a new aerosol submodel for global simulations (v1), Geoscientific Model Development, 3, 391-412, 2010.

Rausch, J., Heidinger, A., and Bennartz, R.: Regional assessment of microphysical properties of marine boundary layer cloud using the PATMOS-x dataset, J. Geophys. Res., 115, doi: 10.1029/2010JD014468, 2010.

Roberts, G., Mauger, G., Hadley, O., and Ramanathan, V.: North American and Asian aerosols over the eastern Pacific Ocean and their role in regulating cloud condensation nuclei, Journal of Geophysical Research-Atmospheres, 111, 2006.

Röckner, E., Brokopf, R., Esch, M., Giorgetta, M., Hagemann, S., Kornblueh, L., Manzini, E., Schlese, U., and Schulzweida, U.: Sensitivity of simulated climate to horizontal and vertical resolution in the ECHAM5 atmosphere model, J. Climate, 19, 3771-3791, 2006.

Rosenfeld, D., Clavner, M., and Nirel, R.: Pollution and dust aerosols modulating tropical cyclones intensities, Atmospheric Research, 102, 66-76, 2011.

Sander, R., Baumgaertner, A., Gromov, S., Harder, H., Joeckel, P., Kerkweg, A., Kubistin, D., Regelin, E., Riede, H., Sandu, A., Taraborrelli, D., Tost, H., and Xie, Z. Q.: The atmospheric chemistry box model CAABA/MECCA-3.0, Geoscientific Model Development, 4, 373-380, 2011.

Schwartz, S. E.: Cloud droplet nucleation and its connection to aerosol properties. In: Nucleation and Atmospheric Aerosols, Wagner, M. K. a. P. E. (Ed.), Elsevier, Oxford, 1996.

Seinfeld, J. H. and Pandis, S. N.: Atmospheric Chemistry and Physics: From Air Pollution to Climate Change, John Wiley & Sons, Inc., Hoboken, New Jersey, 2006.

Smoydzin, L., Teller, A., Tost, H., Fnais, M., and Lelieveld, J.: Impact of mineral dust on cloud formation in a Saharan outflow region, Atmospheric Chemistry and Physics, 12, 11383-11393, 2012.

Sorjamaa, R. and Laaksonen, A.: The effect of H_2O adsorption on cloud drop activation of insoluble particles: a theoretical framework, Atmospheric Chemistry and Physics, 7, 6175-6180, 2007.

Sposito, G.: The Chemistry of Soils, Oxford university Press, 1989.

Stone, E. A., Yoon, S.-C., and Schauer, J. J.: Chemical Characterization of Fine and Coarse Particles in Gosan, Korea during Springtime Dust Events, Aerosol and Air Quality Research, 11, 31-43, 2011.

Sullivan, R. C., Guazzotti, S. A., Sodeman, D. A., and Prather, K. A.: Direct observations of the atmospheric processing of Asian mineral dust, Atmospheric Chemistry and Physics, 7, 1213-1236, 2007.

Sullivan, R. C., Moore, M. J. K., Petters, M. D., Kreidenweis, S. M., Roberts, G. C., and Prather, K. A.: Effect of chemical mixing state on the hygroscopicity and cloud nucleation properties of calcium mineral dust particles, Atmospheric Chemistry and Physics, 9, 3303-3316, 2009.

Tobo, Y., Zhang, D., Matsuki, A., and Iwasaka, Y.: Asian dust particles converted into aqueous droplets under remote marine atmospheric conditions, Proceedings of the National Academy of Sciences of the United States of America, 107, 17905-17910, 2010.

Tost, H., Jockel, P. J., Kerkweg, A., Sander, R., and Lelieveld, J.: Technical note: A new comprehensive SCAVenging submodel for global atmospheric chemistry modelling, Atmos. Chem. Phys., 6, 565-574, 2006.

Tsimpidi, A. P., Karydis, V. A., Pandis, S. N., and Lelieveld, J.: Global combustion sources of organic aerosols: model comparison with 84 AMS factor-analysis data sets, Atmos. Chem. Phys., 16, 8939-8962, 2016.

Tsimpidi, A. P., Karydis, V. A., Pozzer, A., Pandis, S. N., and Lelieveld, J.: ORACLE (v1.0): module to simulate the organic aerosol composition and evolution in the atmosphere, Geoscientific Model Development, 7, 3153-3172, 2014.

Twohy, C. H., Kreidenweis, S. M., Eidhammer, T., Browell, E. V., Heymsfield, A. J., Bansemer, A. R., Anderson, B. E., Chen, G., Ismail, S., DeMott, P. J., and Van den Heever, S. C.: Saharan dust particles nucleate droplets in eastern Atlantic clouds, Geophys. Res. Let., 36, doi: 10.1029/2008GL035846, 2009.

Twomey, S.: Pollution and planetary albedo, Atmospheric Environment, 8, 1251-1256, 1974.

Twomey, S. and Wojciechowski, T. A.: Observations of the Geographical Variation of Cloud Nuclei, Journal of the Atmospheric Sciences, 26, 684-688, 1968.

van der Werf, G. R., Randerson, J. T., Giglio, L., Collatz, G. J., Mu, M., Kasibhatla, P. S., Morton, D. C., DeFries, R. S., Jin, Y., and van Leeuwen, T. T.: Global fire emissions and the contribution of deforestation, savanna, forest, agricultural, and peat fires (1997-2009), Atmos. Chem. Phys., 10, 11707-11735, 2010.

Weber, R. J., Guo, H. Y., Russell, A. G., and Nenes, A.: High aerosol acidity despite declining atmospheric sulfate concentrations over the past 15 years, Nat. Geosci., 9, 282-+, 2016.

Atmospheric
Chemistry
and Physics

Open Access

EGU

Discussions

1034   Wurzler, S., Reisin, T. G., and Levin, Z.: Modification of mineral dust particles by cloud processing
1035   and subsequent effects on drop size distributions, Journal of Geophysical Research-Atmospheres,
1036   105, 4501-4512, 2000.
1037   Xu, L. and Penner, J. E.: Global simulations of nitrate and ammonium aerosols and their radiative
1038   effects, Atmospheric Chemistry and Physics, 12, 9479-9504, 2012.
1039   Yamashita, K., Murakami, M., Hashimoto, A., and Tajiri, T.: CCN Ability of Asian Mineral Dust
1040   Particles and Their Effects on Cloud Droplet Formation, Journal of the Meteorological Society of
1041   Japan, 89, 581-587, 2011.
1042   Yienger, J. J. and Levy, H.: Empirical-model of global soil-biogenic NOx emissions, Journal of
1043   Geophysical Research-Atmospheres, 100, 11447-11464, 1995.
1044   Yin, Y. and Chen, L.: The effects of heating by transported dust layers on cloud and precipitation: a
1045   numerical study, Atmos. Chem. Phys., 7, 3497-3505, 2007.
1046   Zender, C. S. and Kwon, E. Y.: Regional contrasts in dust emission responses to climate, J. Geophys.
1047   Res., 110, doi: 10.1029/2004JD005501, 2005.
1048   Zhang, Y., Zhang, X., Wang, K., He, J., Leung, L. R., Fan, J., and Nenes, A.: Incorporating an
1049   advanced aerosol activation parameterization into WRF-CAM5: Model evaluation and
1050   parameterization intercomparison, Journal of Geophysical Research-Atmospheres, 120, 6952-6979,
1051   2015.
1052   Zhao, C. S., Tie, X. X., Brasseur, G., Noone, K. J., Nakajima, T., Zhang, Q., Zhang, R. Y., Huang, M.
1053   Y., Duan, Y., Li, G. L., and Ishizaka, Y.: Aircraft measurements of cloud droplet spectral dispersion
1054   and implications for indirect aerosol radiative forcing, Geophys. Res. Lett., 33, doi:
1055   10.1029/2006GL026653, 2006.
1056

Atmospheric
Chemistry
and Physics
Discussions

Table 1. Comparison of simulated and observed (Karydis et. al, 2011 and the references therein) cloud droplet number concentrations

Location	Lat.	Long.	Alt.	Time	Observation	Simulation
S. Pacific Ocean			PBL	Annual	40	23
S. Pacific Ocean	20S-35S	135W-175W	PBL	Annual	82	26
Eastern Pacific Ocean	29N-32N	120W-123W	450-850m	July	49-279	133
N. Pacific Ocean	41N	131W	<1500m	April	21-74	51
N. Pacific Ocean			PBL	Annual	64	59
W. of Canary Islands	32N	25W	PBL	July	17	115
N. Atlantic Ocean			PBL	Annual	89	112
S. Atlantic Ocean			PBL	Annual	67	51
S. Indian Ocean			PBL	Annual	42	29
West Australia (remote)	30S-40S	88E-103E	PBL	Annual	107	22
Beaufort Sea (Western Arctic Ocean)	72N-78N	154W-159W	202-1017m	June	178-365	25
Beaufort Sea (Western Arctic Ocean)	70.5N-73N	145N-147N	300-3000m	June	20-225	28
Beaufort Sea (Western Arctic Ocean)	65N-75N	130W-170W	400-4600m	April	48-77	39
Northeast Alaska coast	69N-71N	150W-158W	400-4000m	October	10-30	23
Yellow Sea (Eastern coast of China)	28N-31N	127E-131E	PBL	Annual	30-1000	764
SE Asia coast	10N-40N	105E-150E	PBL	Annual	186 (100-250)	522
NE Asia coast			PBL	Annual	129	768
N. America coast (Pacific)			PBL	Annual	96	91
N. America coast (Pacific)	15N-35N	115W-140W	PBL	Annual	159 (150-300)	190
S. America coast (Pacific)			PBL	Annual	77	75
S. America coast (Pacific)	8S-28S	70W-90W	PBL	Annual	182 (100-300)	186
N. Africa coast (Atlantic)			PBL	Annual	95	123
S. Africa coast (Atlantic)			PBL	Annual	95	107
S. Africa coast (Atlantic)	5S-25S	10W-15E	PBL	Annual	153 (130-300)	189
Eastern N. Atlantic Ocean	50N-55N	25W-30W	800-2200m	April	65-300	39
NW coast of Santa Maria, Azores	37N	25W	550-1000m	June	150 (74-192)	83
Canary Islands Vicinity	28N	16.5W	PBL	June-July	51-256	174
Canary Islands Vicinity	28N	16.5W	PBL	June-July	90-300	174
Atlantic Ocean (W. of Morocco)	34N	11W	PBL	July	77	114
Coast of Oregon	45.5N	124.5W	PBL	August	25-210	124
Key West, FL	24.5N	82W	PBL	July	268-560	318
Bay of Fundy, Nova Scotia, Canada	44N	66W	20-290m	August	61 (59-97)	246
Cornwall Coast (SW UK)	50N	5.5W	450-800m	February	130	602
British Isles, UK	55N	2.5W	Surface	April	172	287
British Isles, UK	51N	6W	Surface	October	119	71
British Isles, UK	53N	9.5W	Surface	December	96	318
SE coast of England	51.5N-52N	1.5E-2.5E	380-750m	September	151-249	1019
Indian Ocean (SW of India)	10S-10N	65E-75E	50-550m	February-March	100-500	520

Atmospheric
Chemistry
and Physics
Discussions

Table 1. Continued

| Location	Lat.	Long.	Alt.	Time	Observation	Simulation
Qinghai Province (Western China)	34N-37N	98E-103E	PBL	Annual	30-700	585
Beijing, China	37N-41N	113E-120E	PBL	Annual	30-1100	1185
NE China (East of Beijing)	39N-40N	117.5E-118.5E	1719-1931m	April-May	200-800	813
Hebei Province (Central Eastern China)	35N-40N	112E-119E	PBL	Annual	30-400	1150
Cumbria, N. England	54.5N	2.5W	Surface	March-April	100-2000	743
Cumbria, N. England	54.5N	2.5W	Surface	May	482-549	840
Koblenz, Germany	50N	7.5E	901-914hPa	May	675-900	1258
Koblenz, Germany	50N	7.5E	945hPa	October	965	1039
Northern Finland	68N	24E	342-572m	Annual	154 (30-610)	332
Kuopio, Finland	62.5N	27.5E	306m	August-November	138	1142
Northern Finland	68N	24E	342-572m	October-November	55-470	336
Cabauw, Netherland	51N	4.5E	PBL	May	180-360	946
Jungfraujoch, Switzerland	46.5N	7.5E	Surface	July-August	112-416	176
Barrow, AK	71.5N	156.5W	389-830m	August	56	47
Barrow, AK	71.5N	156.5W	431-736m	May	222	26
Barrow, AK	71.5N	156.5W	297-591m	June	121	31
Barrow, AK	71.5N	156.5W	393-762m	July	54	29
Barrow, AK	71.5N	156.5W	1059-1608m	September	81	23
Southern Great Plains, OK	36.5N	97.5W	795-1450m	Winter	265-281	341
Southern Great Plains, OK	36.5N	97.5W	343-1241m	Winter	244	341
Southern Great Plains, OK	36.5N	97.5W	985-1885m	Spring	200-219	384
Southern Great Plains, OK	36.5N	97.5W	671-1475m	Spring	203	537
Southern Great Plains, OK	36.5N	97.5W	1280-2200m	Summer	128-159	393
Southern Great Plains, OK	36.5N	97.5W	756-1751m	Summer	131	603
Southern Great Plains, OK	36.5N	97.5W	1030-1770m	Autumn	217-249	505
Southern Great Plains, OK	36.5N	97.5W	404-1183m	Autumn	276	642
Southern Great Plains, OK	36.5N	97.5W	900-800hPa	March	200 (100-320)	563
Southern Great Plains, OK	36.5N	97.5W	300-600m	April	650	1159
Southern Great Plains, OK	36.5N	97.5W	700-1200m	September-October	457	740
Cleveland, OH; Detroit, MI	40N-42.5N	80.5W-85W	300-1000m	August	320-1300	817
Central Ontario, Canada	50N	85W	<2500m	October	147 (119-173)	201
Central Ontario	50N	85W	2000-2100m	Summer	350-360	143
Central Ontario	50N	85W	1300m	Winter	190	112
Upper NY State	44N	75W	1500m	Autumn	240	583
State College, Pennsylvania	41N	78W	1000-1600m	October	388	551
Mount Gibbes, NC	35.5N	82W	Surface	Annual	238-754	392
Cape Kennedy, FL	28.5N	80.5W	600-2800m	August	250-330	134

Atmospheric
Chemistry
and Physics
Discussions

Table 2. Statistical evaluation of EMAC CDNC against 74 worldwide observational datasets derived from in situ measurements and satellite retrievals.

Site Type	Number of datasets	Mean Observed (cm^{-3})	Mean Simulated (cm^{-3})	MAGE (cm^{-3})	MB (cm^{-3})	NME (%)	NMB (%)	RMSE (cm^{-3})
Clean marine	14	86	53	51	-33	60	-39	81
Polluted marine	24	169	296	159	127	94	75	263
Continental	37	339	536	269	198	80	58	358
Total	75	237	369	193	132	82	56	295
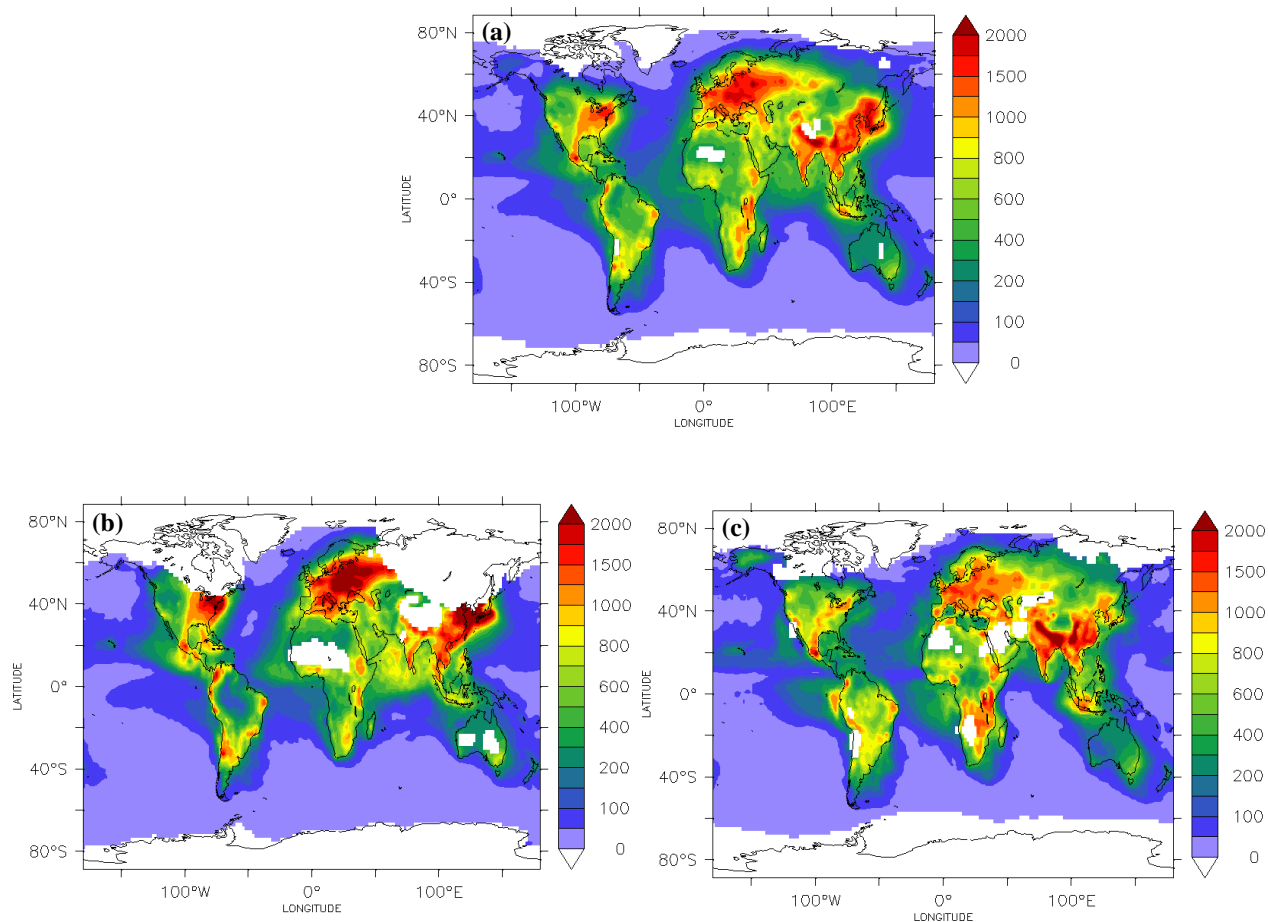
Figure 1: Predicted **(a)** annual, **(b)** DJF, and **(c)** JJA mean cloud droplet number concentrations (cm^{-3}) at the lowest cloud-forming level (940 mb). White color represents areas that are cloud-free or covered by ice clouds.
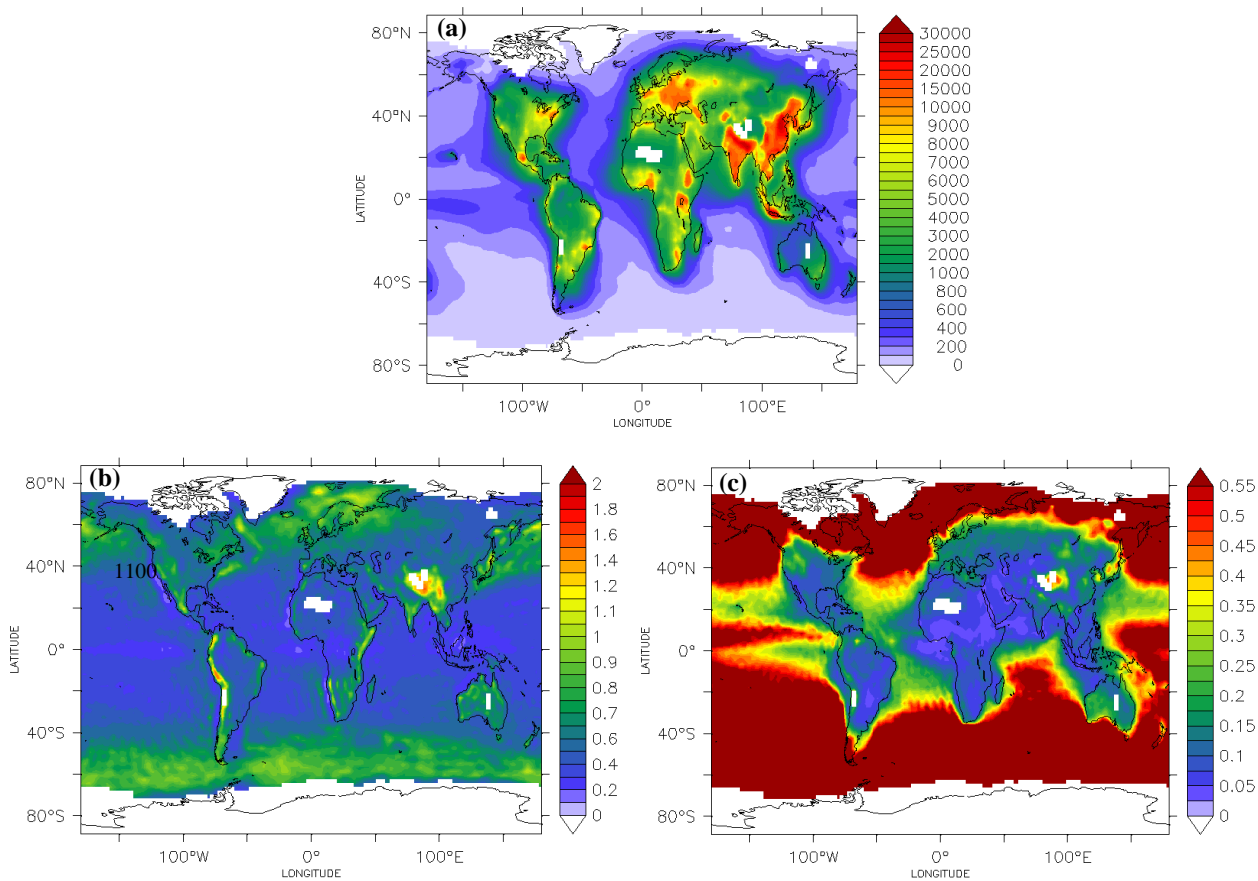
Figure 2: Predicted annual mean **(a)** aerosol number concentration (cm^{-3}), **(b)** large-scale cloud updraft velocity (m s^{-1}), and **(c)** maximum supersaturation (%) at the lowest cloud-forming level (940 mb). White areas correspond to regions where liquid cloud droplets do not form.

Atmospheric
Chemistry
and Physics
Discussions
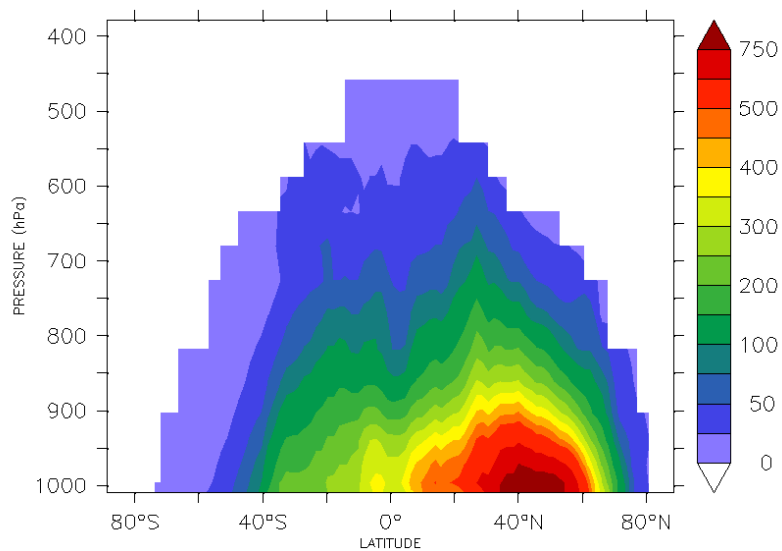
Figure 3: Predicted zonal annual mean cloud droplet number concentration (cm^{-3}).
White areas correspond to regions where liquid cloud droplets do not form.
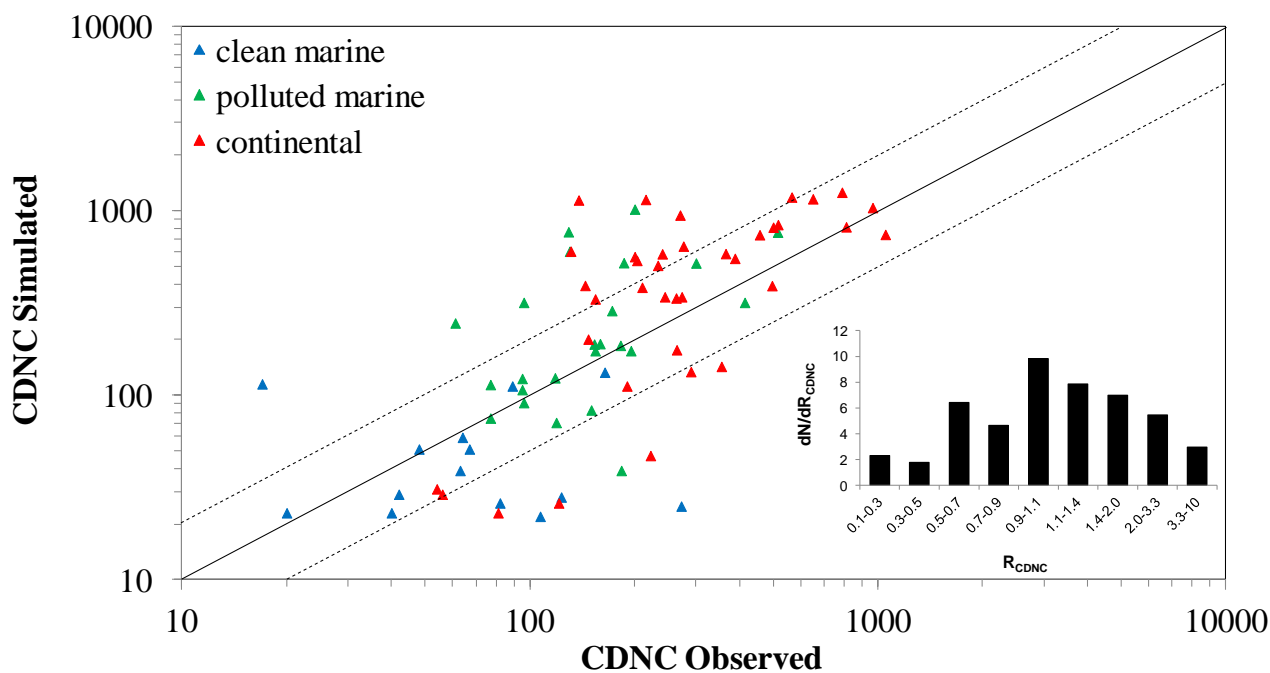
Figure 4: Scatterplot comparing model simulated cloud droplet number concentrations (cm^{-3}) against 74 worldwide observational datasets derived from in situ measurements and satellite retrievals. Also shown are the 1:1, 2:1, 1:2 lines, and the probability distribution of the ratio of the simulated CDNC to the observed CDNC (R_{CDNC}), where N is the number of occurrences in each R_{CDNC} (inset plot).
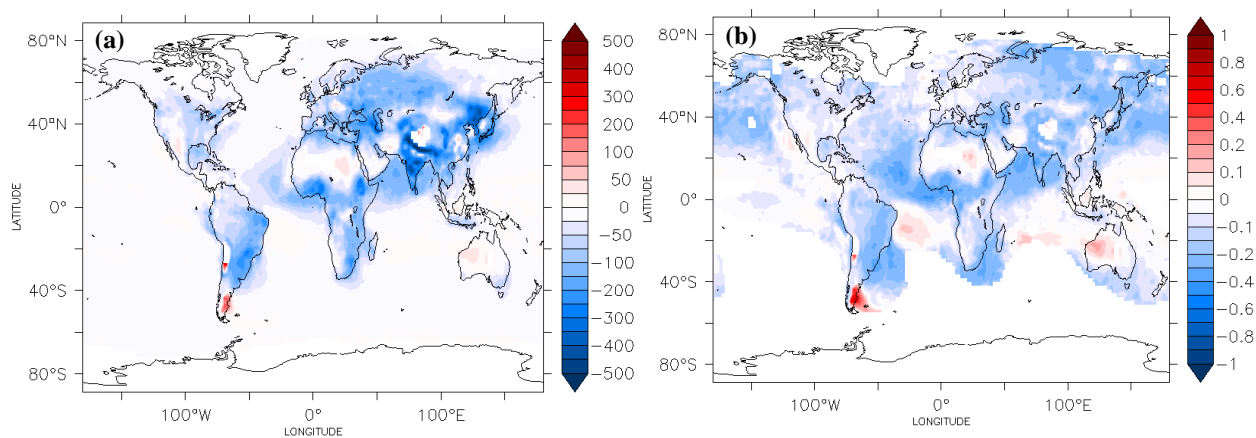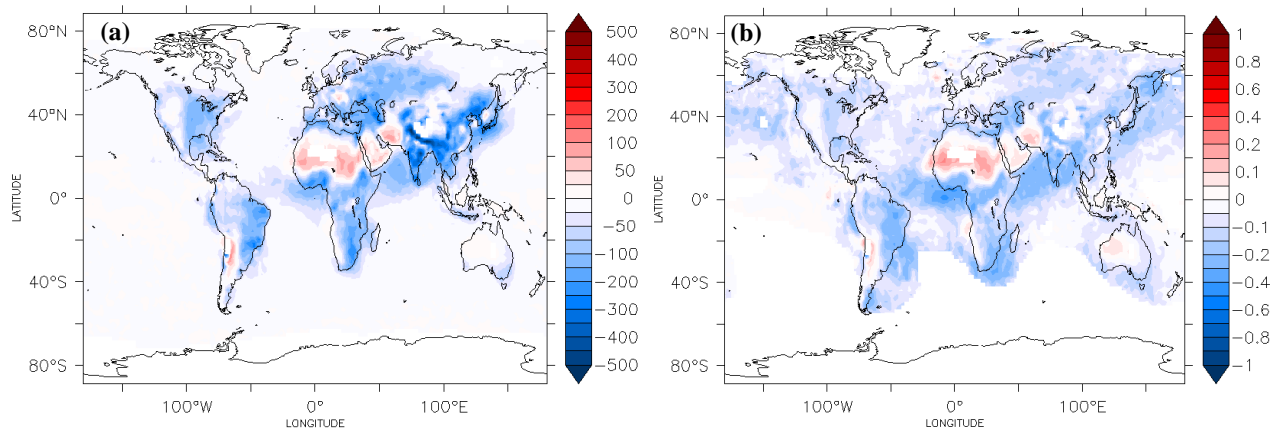
Figure 5: (a) Absolute (in cm^{-3}) and **(b)** fractional annual change of the predicted CDNC (at the lowest cloud-forming level, 940 mb) by switching on/off the mineral dust emissions. A positive change corresponds to an increase from the presence of dust.

Atmospheric
Chemistry
and Physics
Discussions
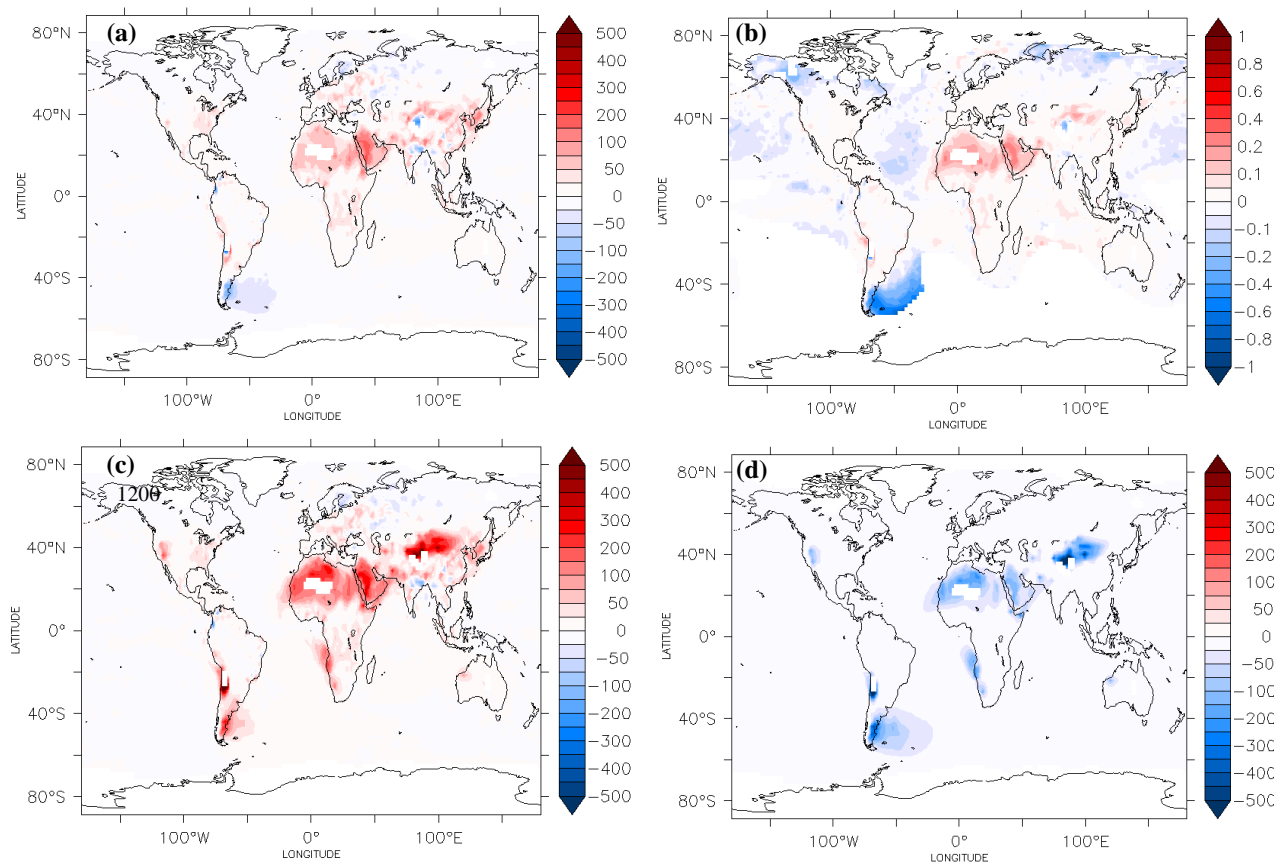
Figure 6: (a) Absolute (in cm^{-3}) and **(b)** fractional annual average change of the predicted total CDNC, and absolute (in cm^{-3}) annual average change of the CDNC from **(c)** soluble and **(d)** insoluble particle modes, by switching on/off the mineral dust chemistry. Concentrations reported at the lowest cloud-forming level (940 mb). A positive change corresponds to an increase from dust–chemistry interactions.

Figure 7: **(a)** Absolute (in cm^{-3}) and **(b)** fractional annual average change of the predicted CDNC (at the lowest cloud-forming level, 940 mb) by switching on/off the FHH adsorption activation physics. A positive change corresponds to an increase from water adsorption on mineral dust.
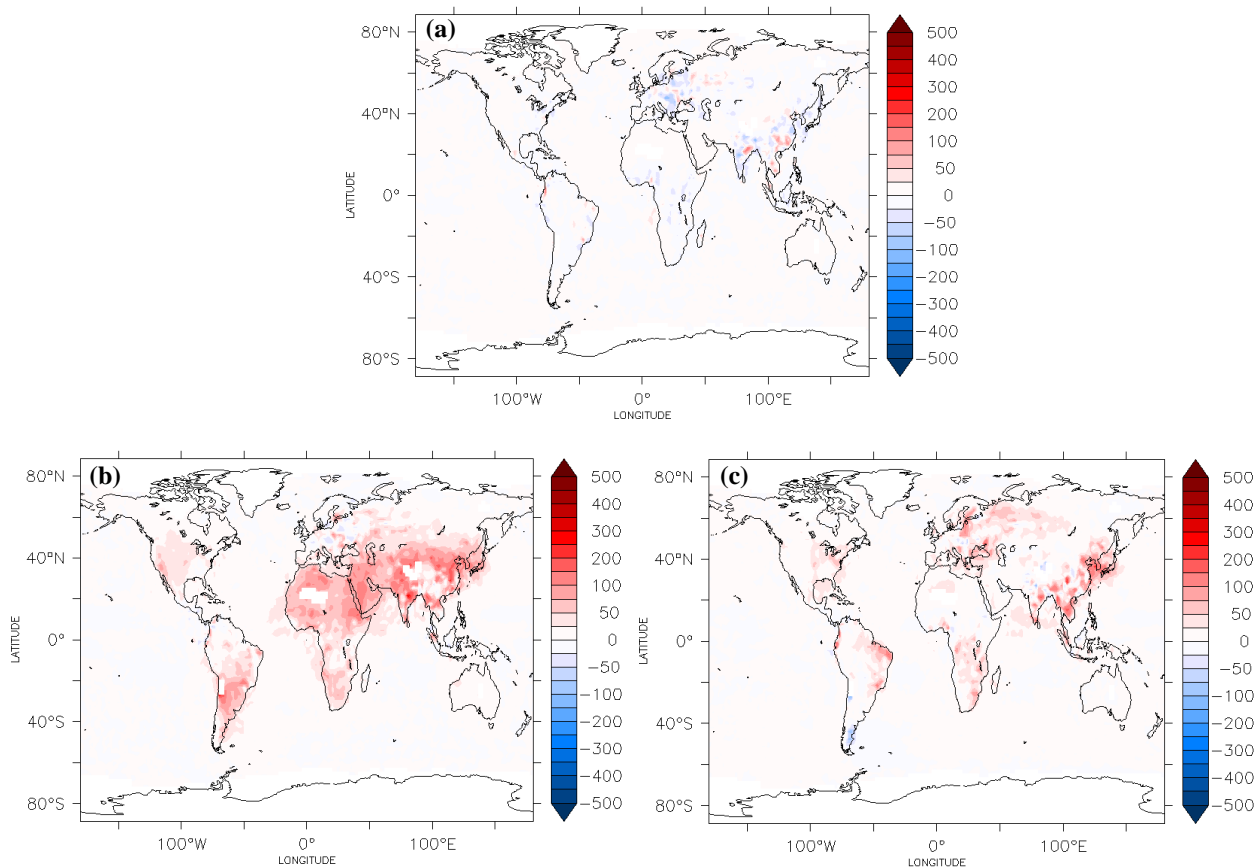
Figure 8: Absolute changes (in cm^{-3}) of the predicted annual average CDNC by **(a)** assuming a globally uniform chemical composition of mineral dust, **(b)** increasing the B_{FHH} hydrophilicity parameter of dust by 10%, and **(c)** reducing mineral dust emissions by 50%. A positive change corresponds to an increase relative to the reference simulation.